

February 2020

Ph.D. Dissertation

**Development and Application of Porous
Carbons from Biomass of Giant
Miscanthus and Algae**

Graduate School of Chosun University

Department of Chemical Engineering

Seokjong Kim

Development and Application of Porous Carbons from Biomass of Giant *Miscanthus* and Algae

거대억새와 미세조류를 이용한 다공성 탄소소재 개발 및 응용

February 25, 2020

Graduate School of Chosun University

Department of Chemical Engineering

Seokjong Kim

Development and Application of Porous Carbons from Biomass of Giant *Miscanthus* and Algae

Supervised by Professor Jae-Wook Lee

A dissertation submitted in partial fulfillment of
the requirements for the Degree of Doctor of
Philosophy in Engineering

October 2019

Graduate School of Chosun University

Department of Chemical Engineering

Seokjong Kim

Approval of the dissertation for Seokjong Kim

Committee Chair	Chosun University	Ph.D./Prof. Jung Heon Lee
Committee	Chosun University	Ph.D./Prof. Hyun-Jae Shin
Committee	Mokpo National University	Ph.D./Prof. Mi-Sug Kim
Committee	Chonam National University	Ph.D./Prof. Kyung-Hee Park
Committee (Dissertation Advisor)	Chosun University	Ph.D./Prof. Jae-Wook Lee

December 2019

Graduate School of Chosun University

Table of Contents

List of Tables	iii
List of Figures	v
Abbreviations, Symbols, and Synonyms	viii
Abstract in English	ix
 Chapter 1. Introduction	 1
1.1 Background of research	1
1.1.1 Biomass	4
1.2 Literature Review	12
1.2.1 Physical and Chemical Activations	12
1.2.2 Microwave-assisted Activation	15
1.2.3 Dissolved Air Flotation	18
1.3 Goal and Outline of This Dissertation	20
 Chapter 2. Theories and Modeling	 23
2.1 Adsorption Kinetics	24
2.1.1 Pseudo-first order equation	24
2.1.2 Pseudo-second order equation	24
2.2 Diffusion models	25
2.3 Equilibrium isotherm models	26
2.3.1 The Langmuir isotherm	26
2.3.2 Freundlich isotherm	27
2.3.3 The Temkin isotherm	27
2.3.4 The Dubinin-Radushkevich isotherm	28
2.4 Physisorption and Chemisorption	29
2.5 Thermodynamic parameters	30

2.6 Model formulation of hydrodynamics for DAF	31
2.6.1 Hydrodynamics	31
2.6.2 Surface forces	33
2.6.3 Collision efficiency for analyzing trajectories	34
Chapter 3. Experimental	38
3.1 Preparation of porous carbon	38
3.1.1 Chemicals	38
3.1.2 Conventional Heating	39
3.1.3 Microwave-assisted Heating	39
3.2 Characterization of porous carbon	40
3.3 Adsorption equilibrium and kinetics measurements	43
3.4 Electrochemical Measurement	43
3.4.1 Preparation of electrode	43
3.5 Dissolved Air Flotation	45
3.5.1 Coagulation and Flocculation	45
Chapter 4. Results and Discussion	48
4.1 Characterization of porous carbon	48
4.2 Adsorption and electrochemical properties	64
Chapter 5. Overall Conclusions	94
Reference	96
Abstract in Korean	106

List of Tables

Chapter 1

Table 1.1	Composition of lignocellulosic feedstocks	7
Table 1.2	Comparison of microwave and conventional heating for activated carbon preparation	15
Table 1.3	Treatment techniques of live algae and dissolved extracellular compounds	18

Chapter 2

Table 2.1	Comparison of physisorption and chemisorption	29
-----------	---	----

Chapter 3

Table 3.1	Chemical properties of Methylene Blue (MB)	38
Table 3.2	Experimental conditions for CGS and DAF	46

Chapter 4

Table 4.1.	Elemental analysis for samples of raw, carbonization and activation	50
Table 4.2.	Elemental analysis for samples of CH-700 and CH-700-H12	52
Table 4.3.	Textural characteristics of untreated carbon and activated carbon	61
Table 4.4.	Textural characteristics of CH-700-H12	63
Table 4.5.	Adsorption kinetics parameters for giant <i>Miscanthus</i> carbon	69
Table 4.6.	Adsorption kinetics parameters for algae biomass carbon	71
Table 4.7.	Adsorption isotherm parameters for <i>Miscanthus Sacchariflorus</i> Carbon	78
Table 4.8.	Thermodynamic parameters for the adsorption of MB onto MS-12-7.5	78
Table 4.9.	Adsorption isotherm parameters for CH-700-H12	79
Table 4.10	Thermodynamic parameters for the adsorption of MB onto CH-700-H12	79
Table 4.11	Capacitance of MS-12-7 for different scan rate	83

Table 4.12	Capacitance of CH-700-H12 for different scan rate	83
Table 4.13	Model Parameters for particle, bubble and water	92

List of Figures

Chapter 1

Figure 1.1	Classification of carbon materials	3
Figure 1.2	Various biomass for the production of carbons	5
Figure 1.3	Scheme for ethanol production from biomass	6
Figure 1.4	Development of biomass supply system on riverside in Korea	8
Figure 1.5	<i>Miscanthus</i> biomass town in Kum river area	9
Figure 1.6	South Korean rivers hit by alga bloom	10
Figure 1.7	Blue-green algae of a) <i>anabaena</i> and b) <i>microcystis</i>	11
Figure 1.8	Physical and chemical activation for producing activated carbon	13
Figure 1.9	Microwave-assisted activation (CH-conventionanl heating, CR: chemical reagents, MW-microwave, PA-physical activation agents) and b) temperature profiles and direction of heat transfer	17
Figure 1.10	Objectives and outline of doctoral thesis	20
Figure 1.11	Peroxide-assisted microactivation for porous biocarbons	21

Chapter 2

Figure 2.1	Model formulation of adsorption and DAF	23
Figure 2.2	Collision and adhesion probability from Navier-Stokes and steam function	32
Figure 2.3.	Extended DLVO theory including hydrophobic interaction	33
Figure 2.4	Schematic of the coordinate system and trajectory of two spheres moving through a fluid	35

Chapter 3

Figure 3.1. Experimental apparatus for conventional carbonization	40
Figure 3.2. Experimental apparatus for microwave activation	41
Figure 3.3 Preparation of biocarbon electrodes	44
Figure 3.4 Experimental apparatus for dissolved air flotation	47

Chapter 4

Figure 4.1 TGA result of a) Giant <i>Miscanthus</i> b) <i>Chlorella ellipsoidea</i>	49
Figure 4.2 SEM images and EDX of Giant <i>Miscanthus</i> a) Raw, b) Carbonization, c) Activation	50
Figure 4.3 SEM images of a) MS-0-0, b) MS-12-7.5	51
Figure 4.4 SEM image and EDX of a) CH-700, b) CH-700-H12	52
Figure 4.5 Particle size distribution of a) MS-0-0, b) MS-12-7.5	53
Figure 4.6 Particle size distribution of CH-700	54
Figure 4.7 XRD patterns of a) CH-700 b) CH-700-H12	55
Figure 4.8 FT-IR spectra of untreated and treated carbons (MS-12-7.5, CH-700-H12)	57
Figure 4.9 Potentiometric titration of biocarbons	58
Figure 4.10 Adsorption-desorption isotherms of a) MS-0-0 and b) MS-12-7.5	60
Figure 4.11 Pore size distribution of MS-0-0 and MS-12-7.5	61
Figure 4.12 Adsorption-desorption isotherms (top) and pore size distribution (bottom) of CH-700	62
Figure 4.13 Effect of (a) impregnation time and (b) microwave radiation time	65
Figure 4.14 Adsorption capacity of methylene blue on algae biomass carbon	66
Figure 4.15 Pseudo-second-order plots of a) MS-0-0, b) MS-12-5, c) MS-12-7.5 and comparison of samples in 10 mg L ⁻¹ MB solution	67

Figure 4.16	Pseudo-second-order kinetic models of a) MS-0-0, b) MS-12-5, c) MS-12.7.5 in different concentration of MB solution	68
Figure 4.17	Adsorption kinetics of methylene blue on untreated carbon and treated carbons a) concentration change over time, b) pseudo-second order kinetic models	70
Figure 4.18	Adsorption isotherms of MS-12-7.5 at different temperatures	74
Figure 4.19	A plot of $\ln K_d$ vs. $\frac{1}{T}$ for the adsorption process of MB on MS-12-7.5	75
Figure 4.20	Adsorption Isotherm of Methylene blue on CH-700-H12 depending on temperatures	76
Figure 4.21	A plot of $\ln K_d$ vs. $\frac{1}{T}$ for the adsorption process of MB on CH-700-H12	77
Figure 4.22	CV curves (top) of MS-12-7.5 electrode at different scan rates of 10, 20, 50, 100 mV s ⁻¹ and the plot of the peak current as a function of the square root of the scan rate (bottom)	84
Figure 4.23	CV curves of CH-700-H12 electrode at different scan rates of 50, 100, 150 and 200 mV s ⁻¹ and the plot of the peak current as a function of the square root of the scan rate (bottom)	85
Figure 4.24	Collision frequency and attachment efficiency as functions of bubble and particles size	88
Figure 4.25	Physical constant for the calculation of electrostatic interaction (V_E), van der Waals dispersion interaction (V_D) and hydrophobic interaction (V_H)	90
Figure 4.26	Potential energy of bubble-particle interaction as a function of distance	91
Figure 4.27	Coagulation and sedimentation of powdered biocarbons	93

Abbreviation, Symblos, and Synonyms

q_e	Amount of sorbate at equilibrium
q_t	Amount of sorbate at time
k_1	Rate constant of the pseudo-first order equation
k_2	Rate constant of the pseudo-second order equation
q	Amount of adsorbate onto the adsorbent at any time
K_i	Diffusion coefficient in the solid
D_i	Diffusion coefficient in the solid.
C_e	Equilibrium concentrations in the liquid phase
q_e	Equilibrium concentrations in the solid phase
q_{\max}	Maximum uptake constant
b	Langmuir sorption constant related to the sorption process energy and the affinity of the binding sites
q_{\max}	Calculated from the intercept
b	Slope of the linear plot of Langmuir isotherm.
C_e	Equilibrium concentration
q_e	Adsorbed amount
K_F	Constants incorporating all parameters
b	Temkin constant related to the heat of adsorption
K_T	Temkin isotherm constant
E	Free energy of sorption per molecule of adsorbate
K_{DR}	Isotherm constant
q_m	Theoretical saturation capacity
ε	Polanyi potential
R	Gas constant
T	Absolute temperature
K_d	Adsorption distribution constant
P_c	Probability of bubble-particle collision
P_a	Probability of adhesion
P_d	Probability of detachment
r_1	Radii of the bubble and the particle
r_2	Radii of the bubble and the particle
Φ	Potential of the inter-particle force

Abstract in English

Development and Application of Porous Carbons from Natural Biomass

Mr. Seokjong Kim

Directed by Ph.D./Prof. Jae-Wook Lee

Department of Chemical Engineering

Graduate School of Chosun University

There is growing interest of the scientific community on production of activated carbon using biocarbon as potential sustainable precursors carbonized from biomass wastes. In general, physical activation and chemical activation are the main methods applied in the activation process. The physical and chemical properties of activated biocarbon can be controlled for multiple applications including water pollution treatment, CO₂ capture, and energy storage. The key parameters of carbonization and activation are the feedstock with different compositions and activation conditions with conventional and microwave heating. Compared to traditional activated carbon, activated biocarbon appears to be a new potential cost-effective and environmentally-friendly carbon materials with great application prospect in many field.

In this study, hierarchical mesoporous carbon with high surface area and controlled pore size was prepared from two biomass of giant *Miscanthus* and algae. The activation was conducted by a simple process that involved H₂O₂ treatment, followed by microwave heating. H₂O₂ treatment time and microwave irradiation time were optimized based on the adsorption capacity of methylene blue dye on biosorbents. The prepared biosorbent samples were characterized employing TG, SEM, XRD, FTIR, BET, and zeta potential measurement for the evaluation of surface area, pore size distribution and surface morphology. The

adsorption equilibrium and kinetic data of methylene blue were fitted with Langmuir and Freundlich isotherm and pseudo second order model kinetic model, respectively. Adsorption isotherm data measured at different temperatures were used for the determination of thermodynamic properties of ΔG^0 , ΔH^0 , and ΔS^0 . Results showed that the adsorption of methylene blue was feasible, spontaneous, and endothermic. The electrochemical properties were measured by cyclic voltammetry and impedance. It was found that microwave-assisted porous carbons exhibited higher adsorption capacity and excellent electrochemical performance due to the well-developed hierarchical pore structures.

On the other hand, the feasibility of a hybrid system consisting of powdered activated carbon (PAC) adsorption and dissolved air flotation (DAF) processes was examined for simultaneous removal of algae (*Anabaena* and *Microcystis*) and their secondary algal metabolites (2-methylisoborneol and geosmin). Before studying the hybrid system, adsorption equilibrium and kinetics of organics (2-methylisoborneol and geosmin) produced from algae on three powdered activated carbons were studied. The flotation efficiency of algae and PAC in DAF process was evaluated with zeta potential measurements. Zeta potential is a key parameter of double layer repulsion for individual particles and can usually be used to interpret the trend of coagulation efficiency. This study focused on the measurement of zeta potential of algae and activated carbon under various experimental conditions including water characteristics (pure water, stream water, reservoir water) and coagulant dose (10~50 mg/L). Results showed that the variation of zeta potential was highly sensitive depending on the water characteristics and coagulation conditions. Zeta potential of two genera of algae (*Anabaena* sp. and *Microcystis* sp.) were changed highly with coagulant dosage, especially. On the basis of DLVO theory and trajectory analysis, bubble-floc collision efficiency simulated in terms of zeta potential was fitted well with removal efficiency of chlorophyll-a from algae particles. It was found that the control of zeta potential was important for effective removal of algae particles. Interestingly, we also found that the agglomerate of bubble and PAC particle can be successfully floated by DAF. In addition, the simultaneous removal of algae and organics (i.e., secondary algal metabolites) dissolved in water can be achieved by using the hybrid system of adsorption/DAF processes.

Chapter 1

Introduction

1.1 Background of research

Carbon materials including carbon black, graphene, carbon nanotubes, glassy carbon, activated carbon, and porous carbon, have been successfully applied in environmental protection and energy storage area because of their structural and functional diversity (**Figure 1.1**). The performance of the adsorption separation and energy storage devices highly depend on the carbon materials with ideal structural design, simple preparation process, specific properties, abundant resource, low-cost and environmental friendliness. To apply energy storage device, carbon materials have higher electronic conductivity, adjustable microstructure and excellent stability [1-5]. It has been known that graphene is generally prepared by chemical vapor deposition using fossil fuel-based molecules of methane, acetylene, and ethylene. Despite of the specific structure and exceptional physicochemical properties of graphene and carbon nanotube, their preparation process is usually complicated and suffers from high cost and very low yield. In addition, although the synthesis of graphene has been achieved in small batches reactor by classical Hummer's method, the strong acid and oxidation agents used in the synthesis process will bring environmental pollution [3].

Thus, renewable raw materials and low-cost preparation method have highly demands for the development of advanced science and technology. Biomass is readily available, renewable, non-toxic and low cost [6]. In addition, the biomass-derived carbon materials have many advantages of high specific surface area, well defined pore size distribution, excellent electric conductivity and easily surface heteroatom doping. Interestingly, biomass-derived carbons for adsorbents and electrodes have attracted much attention because of their structural diversities (i.e., 0D spherical, 1D fibrous, 2D lamellar and 3D spatial

structures) and surface heteroatom doping [7-12]. So far, many biomass precursors including rice husk, waste coffee beans, wood, bamboo and peanut shell have been prepared by pyrolysis, physical and chemical activation, or hydrothermal carbonization. In especial, the biomass-derived carbon electrodes have many advantages including high specific surface area, well defined pore size distribution, excellent electric conductivity and easily modified surface chemistry [13-16]. Surprisingly, numerous biomass-derived carbon materials are naturally porous or unique hierarchical pore structures created by activation process.

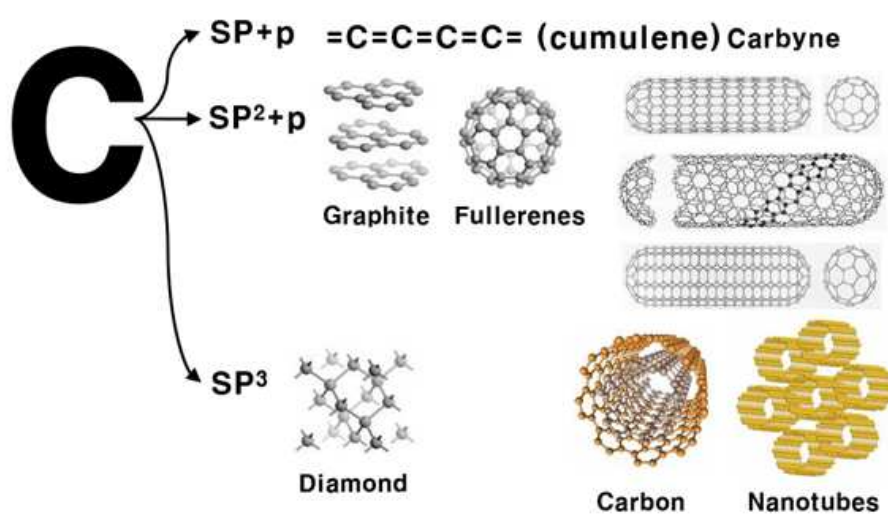


Figure 1.1 Classification of carbon materials

1.1.1 Biomass

Many biomass precursors including rice husk, waste coffee beans, wood, bamboo and peanut shell have been used to prepared porous carbon materials [15-18]. As shown in **Figure 1.2**, Lee et al. reported recently the preparation of bio-carbons from other biomass precursors including corn-grain, Kapok, Hasuo, bean curd dregs, seaweed, coffee grounds and brewery yeast for carbon electrodes of electric double layer capacitors and the adsorption of methane, hydrogen, and volatile organic compounds of benzene and toluene [19-27]. As a continuous work, giant *Miscanthus* and algae biomass were employed in this study for the production of porous carbons.

1.1.1.1 Giant *Miscanthus*

Geodae-Uksae 1 (*Giant Miscanthus*) is a sort genotype of *Miscanthus sacchariflous* (Amur silvergrass) for energy crop [28]. It is approximately twice as tall and thick as common *M. sacchariflorus*. The mass yield of the dry stalk is approximately 30 ton/ha. Geodae-Uksae 1 (*Giant Miscanthus*) grows approximately 4 m tall with an average stalk diameter of 1 cm. As shown in **Figure 1.3**, Many methods are being applied for the energy conversion of Geodae-Uksae 1, including hydrolysis and fermentation for bioethanol production, combustion through pelletization and fast pyrolysis for the production of bio-oil [29-31]. Geodae-Uksae 1 (*Giant Miscanthus*) cultivation and mass-production system is eco-friendly and sustainable for bioenergy was developed in Kum river area of 148 ha from 2011 to 2013 (**Figure 1.4**, **Figure 1.5**). The chemical compositions of lignocellulosic feedstocks including corn stover, switchgrass, *Miscanthus*, reed canary, popular and willow are cellulose, hemicellulose and lignin (**Table 1.1**).

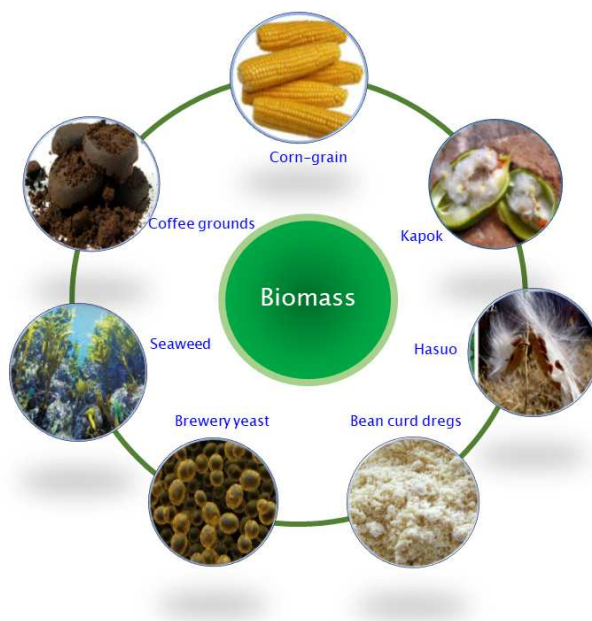


Figure 1.2 Various biomass for the production of carbons

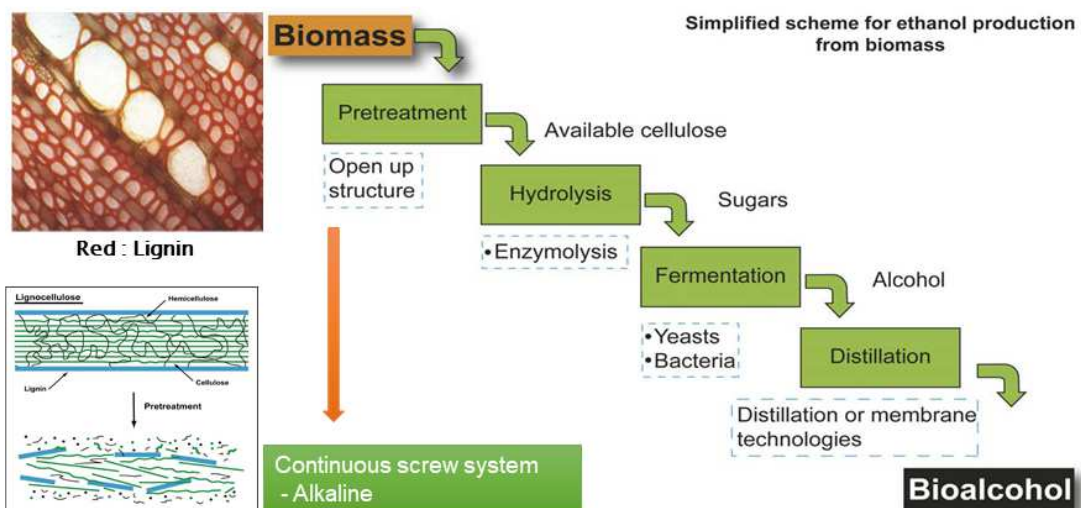


Figure 1.3 Scheme for ethanol production from biomass

Table 1.1 Composition of lignocellulosic feedstocks

Biomass	Carbohydrate			Lignin (%)
	Cellulose (%)	Hemicellulose (%)	Total (%)	
Corn sover	38	26	64	19
Switchgrass	37	29	66	19
Miscanthus	43	24	67	24
Reed canary	24	36	60	-
Forgage sorghum	34	17	51	16
Popular	45	19	64	26
Willow	43	21	64	26



Figure 1.4 Development of biomass supply system on riverside in Korea



Figure 1.5 *Miscanthus* biomass town in Kum river area

1.1.1.2 Algae

The Four Major Rivers Restoration Project in Korea was completed on October 21, 2001. The funding of the project on the Han, Geum, Nakdong and Yeongsan rivers was 22 trillion won (approximately US\$19.3 billion) for the construction of 16 dams and dredged 520 million cubic metres of mud from the river beds for flood prevention. Unfortunately, algal blooms have reappeared in summer and winter causing a major scare over the quality of the country's drinking water (**Figure 1.6**) because of the Four Major Rivers Restoration Project. In especial, algae are most seriously affecting the Nakdong and the Han.

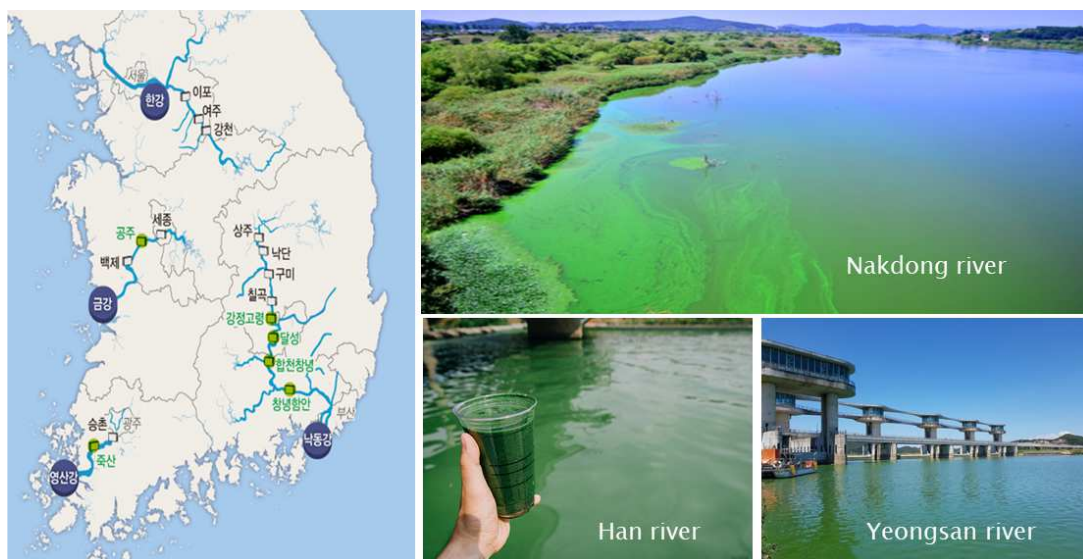


Figure 1.6 South Korean rivers hit by alga bloom

2-methylisoborneol (MIB) and geosmin from blue-green algae in water often produce the musty-earthly taste and odor. Therefore, how to remove taste and odor compounds from drinking water have been received much attention internationally because of significant pollution of water sources. On the other hand, biomass has been widely used to prepare carbons as adsorbents and electrode material, in particular with composition of hemicellulose and lignin. Although algae are not lignocellulose, they involved protein and carbohydrate are also suitable precursors. Interestingly, the conversion of algae into valuable matters would reduce the pollution and create economic benefits [32-38].

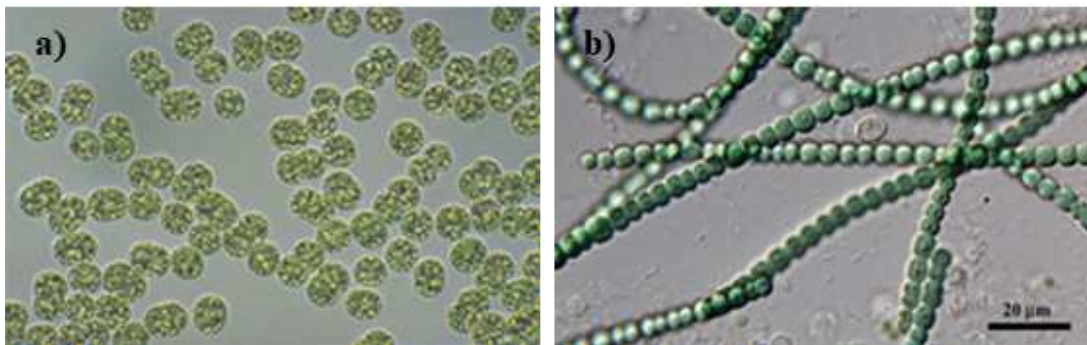


Figure 1.7 Blue-green algae of a) *anabaena* and b) *microcystis*

1.2 Literature Review

1.2.1 *Physical and Chemical Activations*

Activated carbon have been widely used for an many application in separation, decoloration, deodorization, purification, and filtration operations because of large surface area and high mesoporous volume. Major characteristics of the chemical composition, carbonization and activation processes of the biomass, play an important role in the formation of surface area, pores, and pore volume. In general, physical and chemical activations are common methods to prepare activated carbons. Steam, nitrogen, and carbon dioxide are used While, in chemical activation method, a chemical dehydrating agents are employed to activate the biomass (**Figure 1.8**).

Physical activation is normally conducted in two steps of carbonization and activation [39]. Carbonization takes place to eliminate the volatile matters at low temperatures from the raw material. In the next step, the activation of the obtained carbonized (carbon-rich intermediate) material are carried out at much-elevated temperature. The burning of fibrous carbon of biomass can be prevented in the presence of inert gases including steam, N_2 , CO_2 , Ar, or their mixtures for mild reduction of the carbonaceous matter for physical activation. Among inert gases, nitrogen is clean, easy to handle, and available at low-cost. Thus, N_2 is most generally employed as gaseous atmosphere during the activation process. During carbonization, the biomass precursor is pyrolyzed at relatively low temperature to eliminate low molecular weight and volatile organic residues. As a continuous step, activation takes place at temperature of 700 °C to 1100 °C in the presence of supporting gases. They can prevent CO_2 formation and generate pores of diverse sizes in the activated carbon during activation process.

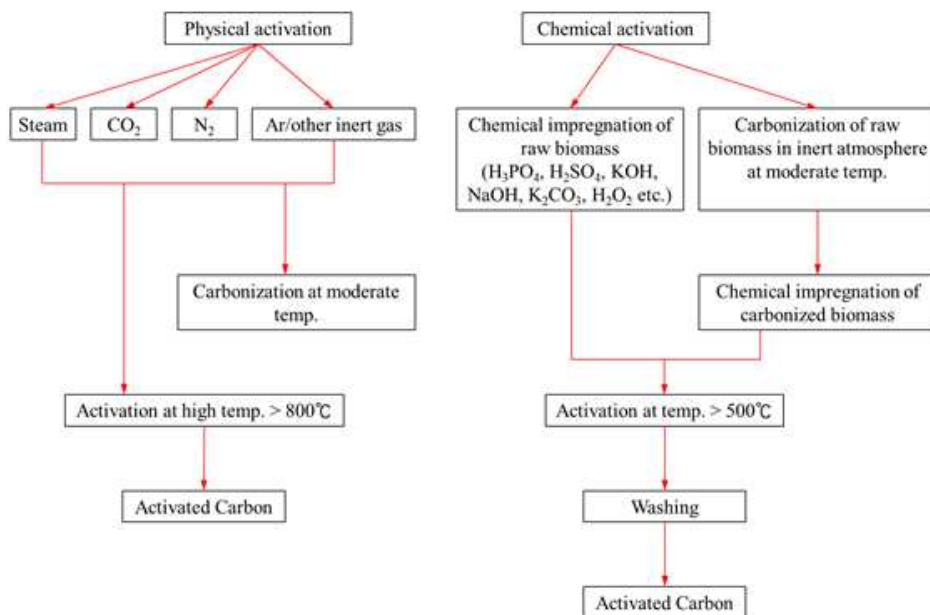


Figure 1.8 Physical and chemical activations for producing activated carbon

Compared to physical activation, chemical activation has numerous advantages. Chemical activation is usually preferred due to the simplicity, shorter activation time, higher yield, lower temperature and incorporation of suitable functional groups such as OH, COO⁻ and C=O, larger surface area, and better development of the porous structure [40-43]. The carbonization and activation processes for chemical activation are combined in one step that saves the heat energy during synthesis. Moreover, chemical activation conducted at a lower temperature compared to physical activation; thus, it also saves energy. Chemically impregnated biomass has higher surface area by heat treatment under an inert atmosphere. The chemical agents (i.e., sulphuric acid, nitric acid, phosphoric acid, zinc chloride, potassium hydroxide, sodium hydroxide, calcium carbonate etc.) are used to generate the pores in the activated carbon using degradation, dehydration, and complexation with organic carbon molecules of precursor materials. Unfortunately, the major disadvantage of the chemical activation process is the cost of chemical agents. To eliminate the surplus unreacted chemicals and chemical by-products, the chemical activation is also required an additional step of flushing activated carbon with hot and cold water. The chemical activation process also has some environmental concern among the researchers over using the dehydrating chemical agents before or after carbonization step. In addition, the environmental friendly chemical dehydrating agent should be used for this uncertainty of the environmentalist. And after cautious treatment of the raw material with chemicals, part of the added chemicals should be recovered.

1.2.2 Microwave-assisted Activation

Compared to conventional heating, microwave-assisted heating is an attractive method offering the internal and volumetric heating [44-48]. The advantages and disadvantages of conventional and microwave-assisted heating are listed in **Table 1.2**

Table 1.2 Comparison of microwave and conventional heating for activated carbon preparation [44]

Heating method	Advantages	Disadvantages
Microwave heating	Fast, volumetric and uniform heating; Non-contact technique; Lower activation temperature; Shorter processing time and energy savings; Temperature gradient from the centre to outer surface; Micro-plasma thermal and catalysis effects; Light components are easily released to create more pores; Improved efficiency; Immediate start-up and shutdown; Improved safety; Smaller equipment size and less feedstock; pre-treatment needed	Hot spots caused by micro-plasma and non-uniformity of materials; Inaccurate temperature measurement and control Thermal runaway; Possible leakage of MW Economics needs to be improved; Process scale-up is not mature.
Conventional heating	Relatively mature process and easy scale-up	Relatively high thermal gradient inside the particle; Non-effectiveness of removal of gaseous products; Carbon deposition and obstruct microporous network; Low pore volume and BET surface area; Distortion and inhomogeneous microstructure; Longer treating time and high cost; Possible fast firing

Microwaves increase the rate of chemical reactions and reduce the energy consumption. The chemical structure, shape and size of microwave-assisted activated carbons are dependent on the number and intensity of the tiny microplasma (small sparks or electric arcs) spots during microwave heating. The appearance of micro-plasmas is limited to tiny space and lasts only for fractional second. The generation of tiny microplasma spots during microwave pyrolysis increases the local temperature resulting in the generation of gases even at low bulk temperatures [45]. Microwave-assisted activation and temperature profiles are shown in **Figure 1.9**. Large amounts of heat can be transferred to the interior of the material. The generation of gases (i.e., CO, CO₂, CH₄, and He) increases the formation of pores in the biocarbons during pyrolysis. Moreover, reaction time is also significantly reduced in microwave heating compared to conventional heating. Recently, microwave heating is applied to prepared activated carbon pretreated with various chemicals. Foo and Hameed have carried out extensive studies on the preparation and of activated carbon from various biomass using chemical agents like KOH, NaOH, and K₂CO₃ [46]. These activated carbons exhibited higher adsorption capacity due to the presence of well-developed pore structure with high surface area and total pore volume. Carbon-based materials are effective microwave absorbers and can be transformed into new materials with modified properties under microwave irradiation. Microwave absorbers may act as catalysts in different heterogeneous reactions.

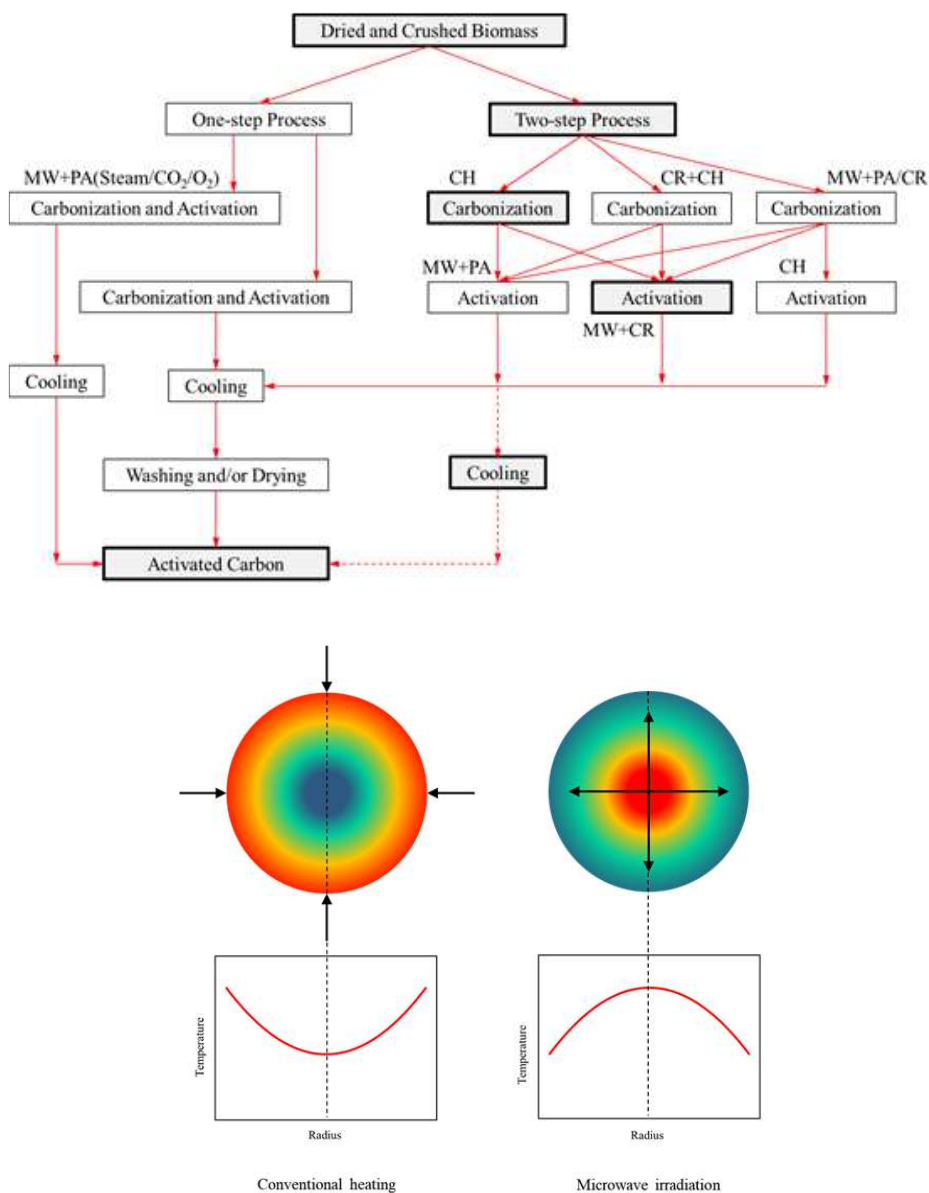


Figure 1.9 a) Microwave-assisted activation (CH-conventional heating, CR: chemical reagents, MW-microwave, PA-physical activation agents) and b) temperature profiles and direction of heat transfer [44]

1.2.3 Dissolved Air Flotation

The Four Major Rivers (i.e., Han, Geum, Nakdong and Yeongsan) Restoration Project in South Korea stimulate the algae bloom seriously. The waters in reservoirs generally have algal particles with low density because of eutrophication. Therefore, the particles are very difficult to remove by the conventional processes of coagulation, flocculation, and sedimentation. More recently, the presence of the musty-earthly taste and odor algal metabolites (i.e., 2-methylisoborneol (MIB) and geosmin) in water treatment causes complaints from consumers. The limiting concentration of musty-earthly odors of MIB and geosmin is as low as 10 ng/L. The major treatment techniques for the removal of algae and extracellular taste and odor compounds (Geosmin and 2-MIB) are listed in **Table 1.3**.

Table 1.3 Treatment techniques of live algae and dissolved extracellular compounds

Removal of Live Algae	Removal or Destruction of Extracellular T&O Compounds
Pre-treatment techniques <ul style="list-style-type: none"> · Coagulation/Flocculation/Sedimentation · Coagulation/Flocculation/Ballasted Flocculation · Coagulation/Flocculation/DAF 	Oxidative Techniques <ul style="list-style-type: none"> · Chlorine · Potassium permanganate · Advanced oxidation · Ozonation
Filtration Processes <ul style="list-style-type: none"> · Granular media filtration · Low pressure membrane filtration · Cartridge and bag filters · Strainers · Reverse osmosis or nanofiltration 	Sorptive Techniques <ul style="list-style-type: none"> · Powdered activated carbon (PAC) · Granular activated carbon (GAC) · Biologically active filtration

Dissolved air flotation (DAF) is an effective separation process of solid/liquid mixtures for low density particles including algae, color, and clay flocs produced from low turbidity water [46,49-58]. However, the removal efficiency of DAF is very limited for the removal of the secondary algal metabolites dissolved in water. DAF processes consist of four unit process of coagulation and flocculation, bubble generation, bubble-floc collision and attachment in a mixing zone, and rising of bubble-floc agglomerates in a flotation tank. When bubble-PAC particles collision results in successful attachment, and bubble-particle agglomerate is positively buoyant, the agglomerate can rise to the top of the liquid column

and collect in a foam layer which can subsequently be skimmed off. Based on the assumption the PAC can be successfully floated by DAF, a combination process of DAF and PAC adsorption seems to be widely applied in water and wastewater treatment. Many works have been conducted on individual process of adsorption and DAF for the removal of MIB and geosmin, and algae, respectively. However, little has been reported on the combination of the two processes of adsorption and DAF.

1.3 Goal and Outline of This Dissertation

The final target of this study is to develop a promising method for producing hierachical mesoporous activated carbon from raw biomass materials of giant *Miscanthus* and algae (**Figure 1.10**) by peroxide-assisted microwave activation for environmental protection technologies (**Figure 1.11**).

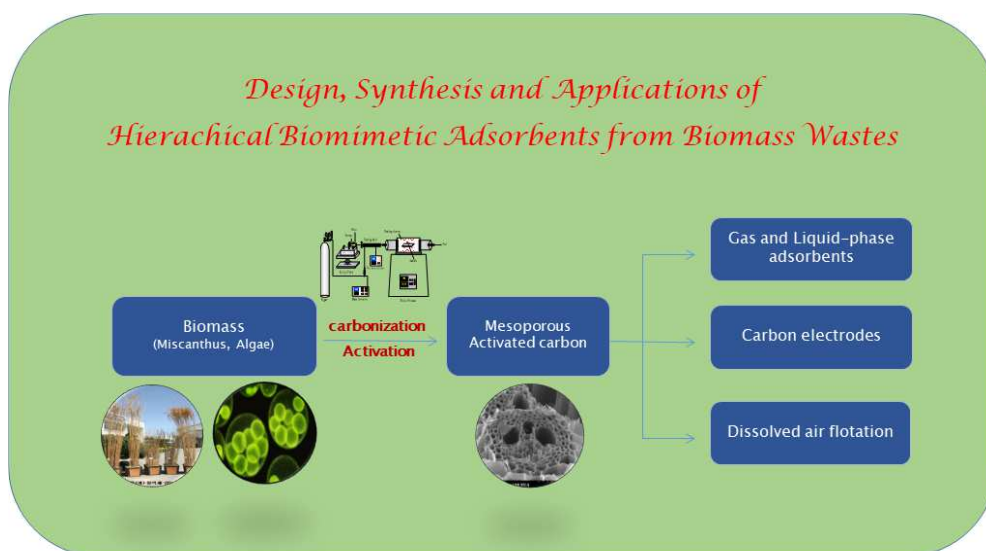


Figure 1.10 Objectives and outline of doctoral thesis

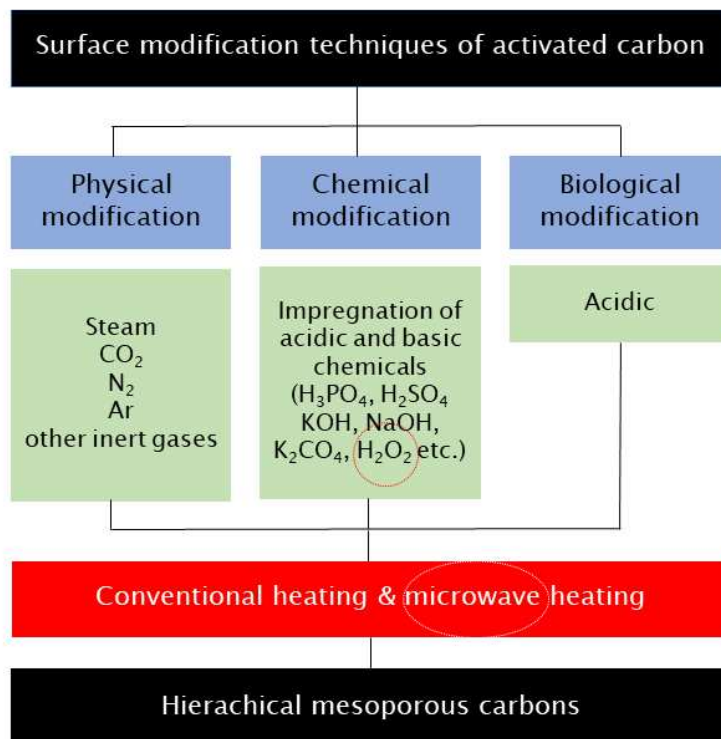
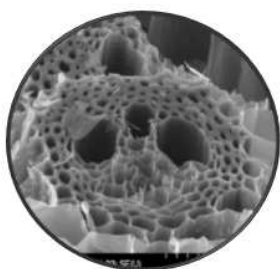


Figure 1.11 Peroxide-assisted microactivation for porous biocarbons

The outline of this thesis is given as follows.

Chapter 1: Introduction

The different physiochemical properties of the biocarbons prepared from giant *Miscanthus* and algae are discussed in this chapter. In addition, information about different processes of physical, chemical, and microwave activations for preparation of activated carbons are explained along with the advantages of using activated carbons in various modern applications due to textual and surface characteristics of the activated carbons.

Chapter 2: Theories and modeling

Different adsorption isotherm and kinetics models, thermodynamic properties are introduced in this chapter. In addition, collision efficiency for analyzing trajectories in DAF processes are introduced.

Chapter 3: Experimental

The preparation and characterization of hierarchical porous carbons by different activation processes using conventional heating and microwave heating and the optimal characteristics of activated carbons are discussed in this chapter for various different applications.

Chapter 4: Results and discussion

The physiochemical properties are evaluated based on the results of various analysis including TG/DTA, SEM, TEM, particle size distribution, FT-IR, BET and zeta potential. The adsorption and electrochemical properties are discussed in detail. In addition, the experimental and theoretical analysis for flotation efficiency of porous activated carbon were systematically studied for simultaneous removal of dissolved organics and algae particles in water by dissolved air flotation processes.

Chapter 5: Overall conclusion and recommendation

The overall conclusion and recommendations are summarized in detail.

Chapter 2

Theories and Modeling

Before studies on the hybrid system of adsorption and dissolved air flotation (DAF), adsorption characteristics (i.e., equilibrium and kinetics) and thermodynamic properties of dissolved organics on PAC particle, as well as hydrodynamics and surface forces of bubble-particle interaction were theoretically analyzed.

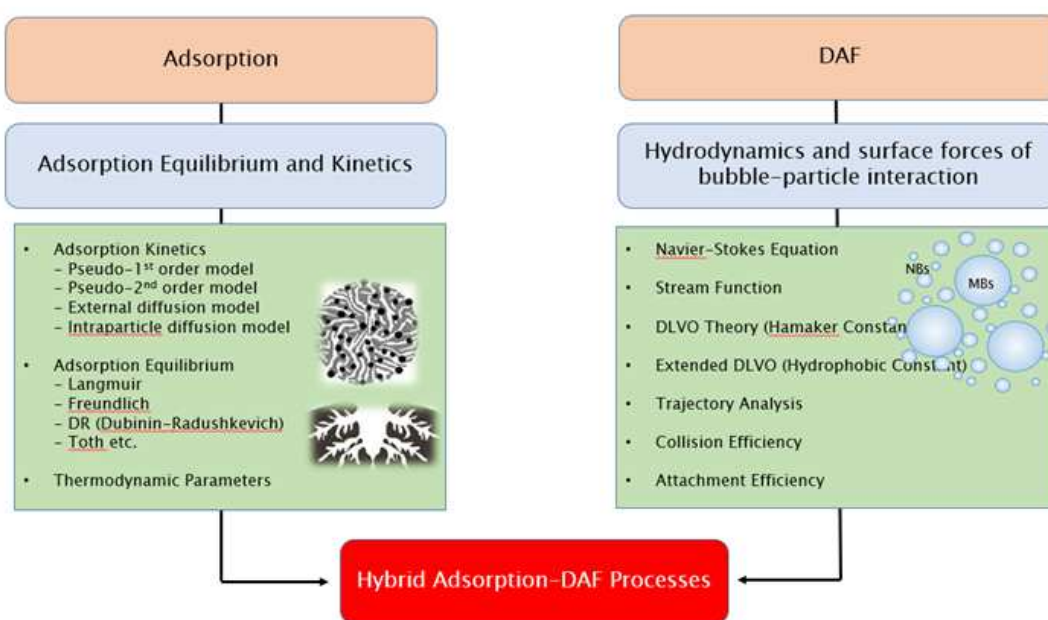


Figure 2.1 Model formulation of adsorption and DAF

2.1 Adsorption Kinetics

The kinetic models of pseudo-first-order and pseudo-second-order were applied to examine the rate controlling step of biocarbons in the adsorption process. In addition, the external mass transfer diffusion model and intraparticle mass transfer diffusion model were used to determine the diffusion mechanism of the adsorption system.

2.1.1 Pseudo-first order equation

The pseudo-first order equation is generally written as [60]:

$$\frac{dq_t}{dt} = k_1(q_e - q_t) \quad (\text{Eq. 2.1})$$

where q_e (mg g⁻¹) is the amount of sorbate at equilibrium, q_t (mg g⁻¹) is the amount of sorbate at time t (min), and k_1 (min⁻¹) is the rate constant of the pseudo-first order equation.

2.1.2 Pseudo-second order equation

The pseudo-second order equation is as follow relationship [61]:

$$\frac{dq_t}{dt} = k_2(q_e - q_t)^2 \quad (\text{Eq. 2.2})$$

where k_2 (g mg⁻¹min⁻¹) is the rate constant of the pseudo-second order equation .

2.2. Diffusion models

The adsorption of adsorbate on the adsorbent is carried out by diffusion or mass transfer process based on the three steps as follows:

Step 1. External diffusion

Mass transfer from the boundary liquid film to the surface of the solid.

Step 2. Internal diffusion

Mass transfer from the surface to the intra-particle active sites.

Step 3. Adsorption

Uptake of adsorbate by complexation, sorption or intra-particle precipitation

Weber and Morris addressed the intraparticle diffusion model which has been used in several studies. The initial rate of intraparticle diffusion is determined by linear plot of the curve expressed by:

$$q = K_i t^{0.5} \quad (\text{Eq. 2.3})$$

where q (mg g^{-1}) is the amount of adsorbate onto the adsorbent at any time (s) and K_i ($\text{mg g}^{-1} \text{s}^{-0.5}$) is the diffusion coefficient in the solid .

Urano and Tachikawa reported the intraparticle diffusion model obtained from the assumption that the adsorption rate is independent of the stirring speed and external diffusion is negligible relative to the low overall adsorption rate. The final model equation is as follows:

$$-\ln \left[1 - \left(\frac{q}{q_e} \right)^2 \right] = \frac{4\pi^2 D_i t}{d_p^2} \quad (\text{Eq. 2.4})$$

where D_i ($\text{m}^2 \text{s}^{-1}$) is the diffusion coefficient in the solid.

2.3. Equilibrium isotherm models

An adsorption isotherm is the relationship between the adsorption capacity of adsorbent and the adsorbate concentration remaining in the solution. The adsorption isotherms are the most important information to understand the mechanism on the sorption process. There are many isotherm equations for analyzing experimental adsorption equilibrium data. The information of the adsorption mechanism and the surface properties and affinity of the sorbent are generally obtained from the isotherm parameters and underlying thermodynamic assumptions of these equilibrium models. In this work, three important models (i.e. Langmuir, Freundlich, Temkin and Dubinin-Radushkevich) were selected for evaluation purposes .

2.3.1. The Langmuir isotherm

The Langmuir model is described by the following equation [63]:

$$q_e = \frac{q_{\max} b C_e}{1 + b C_e} \quad (\text{Eq. 2.5})$$

where C_e is the equilibrium concentrations in the liquid phase (mg L^{-1}), q_e is the equilibrium concentrations in the solid phase (mg g^{-1}), q_{\max} is the maximum uptake constant (mg g^{-1}) and b is also a Langmuir sorption constant related to the sorption process energy and the affinity of the binding sites (L mg^{-1}). The adsorption capacities and Langmuir constants can be estimated by the linear plot of Langmuir isotherm. This isotherm is given by the following expression:

$$\frac{1}{q_e} = \frac{1}{q_m b C_e} + \frac{1}{q_m} \quad (\text{Eq. 2.6})$$

where q_{\max} and b are calculated from the intercept and slope of the linear plot of Langmuir isotherm.

2.3.2. Freundlich isotherm

The Freundlich isotherm is an empirical model employed to describe heterogeneous systems. The Freundlich equation [64] is as follows:

$$q_e = K_F C_e^{1/n} \quad (\text{Eq. 2.7})$$

where C_e is the equilibrium concentration (mg L^{-1}), q_e is the adsorbed amount (mg g^{-1}), K_F and n are constants incorporating all parameters affecting the adsorption process, such as adsorption capacity and intensity, respectively. The linearized form of Freundlich adsorption isotherm is used to evaluate the sorption data and is represented as:

$$\ln q_e = \ln K_F + \frac{1}{n} \ln C_e \quad (\text{Eq. 2.8})$$

where K_F and n are calculated from the intercept and slope of the Freundlich plot of (Eq. 2.8).

2.3.3. The Temkin isotherm

The Temkin isotherm model considers the influence of adsorbate-adsorbate interaction on the adsorption process based on the assumption that the heat of adsorption of all molecules on the surface decreases linearly with increase of surface coverage. The Temkin equation describes the behaviors of many adsorption systems on heterogeneous surfaces in the coverage region $0.2 < \theta < 0.8$. This isotherm is:

$$q_e = \frac{RT}{b} \ln K_T + \frac{RT}{b} \ln C_e \quad (\text{Eq. 2.9})$$

where b is a Temkin constant related to the heat of adsorption (J mol^{-1}) and K_T is the Temkin isotherm constant (L g^{-1}). K_F and n are calculated from the intercept and slope

of the Temkin plot of (Eq. 2.9).

2.3.4. The Dubinin–Radushkevich isotherm

The Dubinin–Radushkevich (D–R) isotherm is commonly used to describe the adsorption mechanism with Gaussian energy distribution onto heterogeneous surfaces. The model is given by the following equation:

$$q_e = q_m e^{-K_{DR}\epsilon^2} \quad (\text{Eq. 2.10})$$

$$E = \frac{1}{\sqrt{2K_{DR}}} \quad (\text{Eq. 2.11})$$

$$\epsilon = RT \ln \left(1 + \frac{1}{C_e} \right) \quad (\text{Eq. 2.12})$$

where E is the mean free energy (kJ mol^{-1}) of sorption per molecule of adsorbate, K_{DR} is an isotherm constant ($\text{mol}^2 \text{J}^{-2}$), q_m is the theoretical saturation capacity (mg g^{-1}), ϵ is the Polanyi potential (mg L^{-1}), R ($\text{J mol}^{-1} \text{K}^{-1}$) is the gas constant and T (K) is the absolute temperature. The parameter E gives information about the sorption mechanism of chemisorption and physisorption. When the values of E is between 8 and 16 kJ mol^{-1} , the sorption process occurs via chemisorption [67], while for values of $E < 8 \text{ kJ mol}^{-1}$, the sorption process is mainly of physical adsorption [68].

2.4. Physisorption and Chemisorption

It is meaningful to distinguish between physisorption involving only relatively weak intermolecular forces and chemisorption involving essentially the formation of a chemical bond between the adsorbate molecules on the adsorbent surfaces. Although the distinction is conceptually useful there are many intermediate cases. The general features are listed in **Table 2.1**.

Table 2.1 Comparison of physisorption and chemisorption

	Physisorption	Chemisorption
Adsorbent	All solid	Some solids
Adsorbates	All gases below the critical point, intact molecules	Some chemically reactive gases, dissociation into atoms, ions, radicals
Temperature range	Low temperatures	Generally high temperature
Heat of adsorption	Low, ~heat of condensation (typical $\Delta H_{\text{ads}} = -20 \text{ kJ mol}^{-1}$)	High, ~heat of reaction ($\Delta H_{\text{ads}} = -200 \text{ kJ mol}^{-1}$) exothermic
Rate	Very fast	Strongly temp dependent
Activation energy	No barrier activation Barrier, low	Generally high
Surface coverage	Multilayer	Monolayer
Reversibility	High reversible	Often irreversible

2.5. Thermodynamic parameters

To understand the adsorption characteristics of biocarbons, thermodynamic parameters of free energy change, enthalpy change, and entropy change of adsorption can be calculated as follows [70-71]:

$$K_d = \frac{q_e}{C_e} \quad (\text{Eq. 2.13})$$

where K_d is the adsorption distribution constant. The values of ΔG^0 (J mol^{-1}), ΔH^0 (J mol^{-1}) and ΔS^0 ($\text{J mol}^{-1} \text{ K}^{-1}$) are evaluated from the following equations:

$$\Delta G^0 = -RT \ln K_d \quad (\text{Eq. 2.14})$$

$$\Delta G^0 = \Delta H^0 - T\Delta S^0 \quad (\text{Eq. 2.15})$$

$$\ln K_d = -\frac{\Delta H^0}{R} \frac{1}{T} + \frac{\Delta S^0}{R} \quad (\text{Eq. 2.16})$$

where T (K) is the absolute temperature and R ($\text{J mol}^{-1} \text{ K}^{-1}$) is the universal gas constant. The values of ΔH^0 and ΔS^0 can be calculated from the slope and intercept of the $\ln K_d$ vs. $1/T$ plot of (Eq. 2.16).

2.6. Model formulation of hydrodynamics for DAF

2.6.1. Hydrodynamics

For model formulation of DAF process, the bubble-particle interaction is generally divided into three processes of collision, adhesion and detachment. The hydrodynamics of bubble-particle collision has been extensively investigated. However, the adhesion and detachment are less studied because those processes are highly dependent on the chemistry of the system. The probability of bubble-particle aggregates can be given by

$$P = P_c P_a (1 - P_d) \quad (\text{Eq. 2.17})$$

where P_c is the probability of bubble-particle collision, P_a is the probability of adhesion, and P_d is the probability of detachment. For the low inertia, P_d of fine particle can be negligibly small. Thus, the Eq. 2.17 becomes:

$$P = P_c P_a \quad (\text{Eq. 2.18})$$

where P_c is determined by the hydrodynamics of the system. The probability of bubble-particle collision is highly affected by the particle size, bubble size and turbulence of the system. The probability of adhesion (P_a) is influenced by the hydrodynamics and also the surface chemistry involved. Recently the probability of bubble-particle collision and attachment was derived by Yoon based on solving the Navier-Stokes [76]. In addition, Yoon and Luttrell derived a stream function for the intermediate Reynolds number range [77]. They obtained an expression for the probability of collision and attachment using Navier-Stokes and stream function (**Figure 2.2**).

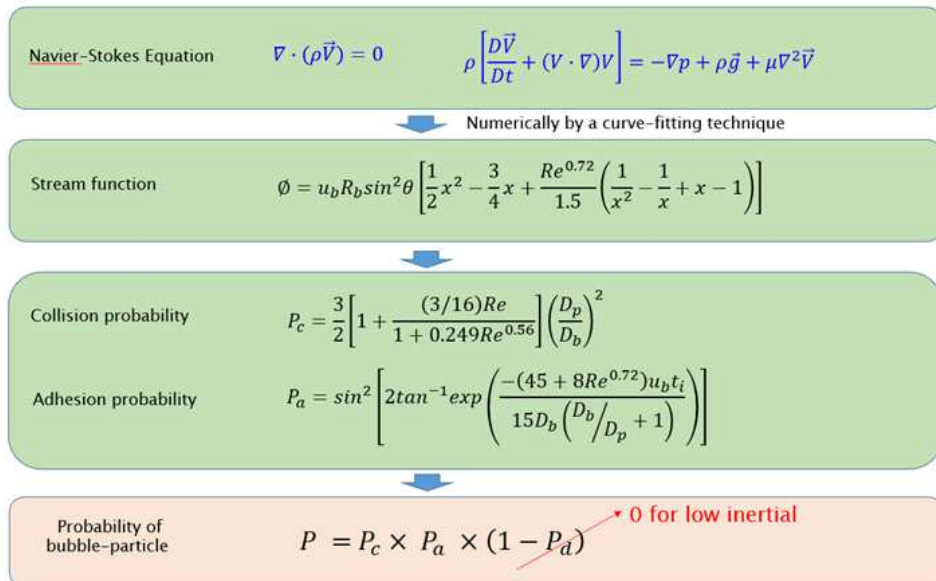


Figure 2.2 Collision and adhesion probability from Navier-Stokes and stream function

2.6.2. Surface forces

Both the particles and bubbles are negatively charged in many flotation systems [76-87]. The classical DLVO theory considers only the electrostatic and dispersion forces to describe the interaction. Recently, Yoon et al. [76] reported the extended DLVO theory which includes the contributions from the hydrophobic interactions between bubble and particle (**Figure 2.3**).

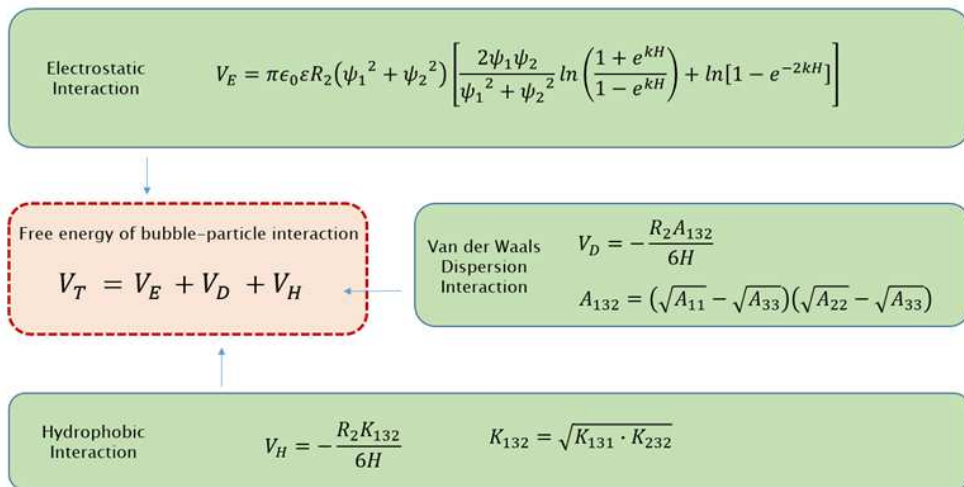


Figure 2.3. Extended DLVO theory including hydrophobic interaction

2.6.3. Collision efficiency for analyzing trajectories

Trajectory analysis is performed to evaluate the collision efficiency of bubble and particle. The collision efficiency of a bubble particle interaction has usually been expressed as follow:

$$E_c = \frac{X_c}{(r_1 + r_2)} \quad (\text{Eq. 2.19})$$

where, r_1 and r_2 are the radii of the bubble and the particle, and $X = X_c$ is the horizontal displacement of the critical trajectory from the vertical axis of the bubble at an infinite distance upstream (**Figure 2.4**). Many researchers have studied the determination of X_c so far. A mathematical model to perform a trajectory analysis was formulated by Leppinen to calculate collision efficiencies between the rising bubble and falling particle [77-78].

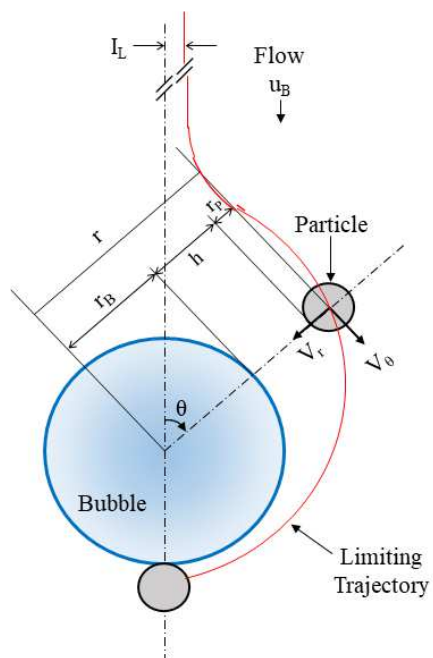


Figure 2.4 Schematic of the coordinate system and trajectory of two spheres moving through a fluid.

The model was formulated by incorporating the hydrodynamics of two particle interactions with interparticle forces. Also, the bubble and particle concentrations are sufficiently small so that higher order interactions are negligible. The governing model equations are as follows [78]:

$$V_{12}(r) = \left[\frac{rr}{r^2} L(s, \lambda, \gamma) + \left(I - \frac{rr}{r^2} \right) M(s, \lambda, \gamma) \right] \cdot V^{(0)_{12}} - \frac{a_1 + a_2}{6\pi\mu a_1 a_2} \left[\frac{rr}{r^2} G(s, \lambda) + \left(I - \frac{rr}{r^2} \right) H(s, \lambda) \right] \cdot \nabla \Phi \quad (\text{Eq. 2.20})$$

where, Φ is the potential of the inter-particle force. Ho et al. [80] used the van der Waals potential (Φ_{VDW}) for the interaction between two spheres.

$$p < 1, \Phi_{VDW} = - \frac{A\lambda}{3(1+\lambda)^2(s-2)(1+1.7692p)} \quad (\text{Eq. 2.21})$$

$$p \geq 1, \Phi_{VDW} = - \frac{A\lambda}{3(1+\lambda)^2(s-2)} \left(\frac{2.45}{5p} - \frac{2.17}{15p^2} + \frac{0.59}{35p^3} \right)$$

The electrostatic potential (Φ_{ELEC}) for the interaction attributed to thin overlapping double layers was used as the model:

$$\Phi_{ELEC} = \frac{\varepsilon a_1 a_2}{4(a_1 + a_2)} \left[2\zeta_1 \zeta_2 \ln \left(\frac{1 + e^{-kh}}{1 - e^{-kh}} \right) + (\zeta_1^2 + \zeta_2^2) \ln(1 - e^{-2kh}) \right] \quad (\text{Eq. 2.22})$$

The relative motion trajectory is determined by the decomposing Eq. (2.22) into radial and tangential components as shown in **Figure 2.4**.

$$V_r = \frac{ds}{dt} = -\cos\theta L(s, \lambda) V_{12} - \frac{D_{12}}{KT} G(s, \lambda) \nabla \Phi_{12} \quad (\text{Eq. 2.23})$$

$$V_\theta = s \frac{d\theta}{dt} = M(s, \lambda) \sin\theta V_{12} \quad (\text{Eq. 2.24})$$

From Eq. 2.23 and Eq. 2.24, the governing equation of the streamline method for analyzing the trajectory can be given as follows:

$$\frac{dr}{d\theta} = s \frac{V_r}{V_\theta} = \frac{-\cos\theta L(s, \lambda) V_{12} - \frac{D_{12}}{KT} G(s, \lambda) \nabla \Phi_{12}}{M(s, \lambda) \sin\theta V_{12}} \quad (\text{Eq. 2.25})$$

The model parameters of Eqs. (2.21)~(2.25) are described in detail [78]. Numerical solution of Eq. (2.25) was solved as a function of time using Matlab software.

Chapter 3

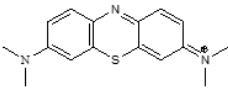
Experimental

3.1 Preparation of porous carbon

3.1.1 Chemicals

Giant *Miscanthus* used in this experiment was provided by the Korea Rural Development Administration, and *Chlorella ellipsoidea* used concentrated culture medium. Giant *Miscanthus* was thoroughly washed and dried. After washing, centrifugation, and filtration of *Chlorella ellipsoidea*, the remainders were freeze-drying for 12 h. Methylene blue, a monovalent cationic dye was selected as the model adsorbate in this work. Methylene blue was bought from Sigma-Aldrich. The chemical properties of methylene blue is listed in **Table 3.1**. All solutions were prepared using distilled water. All other chemicals were of analytical grade and used as received.

Table 3.1 Chemical properties of Methylene Blue (MB)

Property	MB
Chemical formular	$C_{16}H_{18}N_3SCl$
Molecular weight ($g \cdot mol^{-1}$)	284.29
Molar volume ($cm^3 \cdot mol^{-1}$)	241.9
Width (\AA)	14.3
Depth (\AA)	6.1
Thickness (\AA)	~ 4
UV anlysis (nm)	661
Chemical structure	

3.1.2 Conventional Heating

The biomass materials were air-dried and subsequently oven-dried at 110 °C for 24 h to remove the moisture content. They were transferred to furnace for pre-carbonized at 100 °C for 1 h and further carbonized at 700, 800 and 900 °C for 1 h at the heating rate of 5 °C min⁻¹ under N₂ atmosphere. The experimental apparatus for conventional heating is shown in **Figure 3.1**.

3.1.3 Microwave-assisted Heating

Porous carbons prepared from giant Miscanthus and Chlorella ellipsoidea were used as the starting material for activation. A 2.0 ~ 3.0 g of the prepared porous carbon was added to 30 ~ 45 mL of hydrogen peroxide solution for 12 h. Then reactents were cooled to room temperature and then dried at 110 °C for 4 h. A 1.5 ~ 2.5 g of dried sample was placed in quartz tube inside the microwave reactor. The microwave-assisted heating was carried out with 5 ~ 10 min microwave irradiation under power 700 W and N₂ flow (200 mL min⁻¹). Then cooled down and the obtained sample was named as MS-X-Y (X and Y denote immersion and irradiation times), and CH-XX-YY (XX and YY denote carbonization temperature and immersion times). Experimental apparatus for microwave activation was shown in **Figure 3.2**.

3.2 Characterization of porous carbon

Dried giant *Miscanthus* and *Chlorella ellipsoidea* biomass samples were preheated according to the methodology followed by to further reduce the moisture content. After such conditioning of biomass samples, TGA was carried out using a TA Instruments TGA2050, which is able to supply a continuous measurement of sample mass as a function of time or temperature. Samples were placed in a pottery crucible and heated at three heating rates ($5\text{ }^{\circ}\text{C min}^{-1}$) from ambient to $800\text{ }^{\circ}\text{C}$. This heating was carried out under N_2 atmosphere to carry out the combustion process.

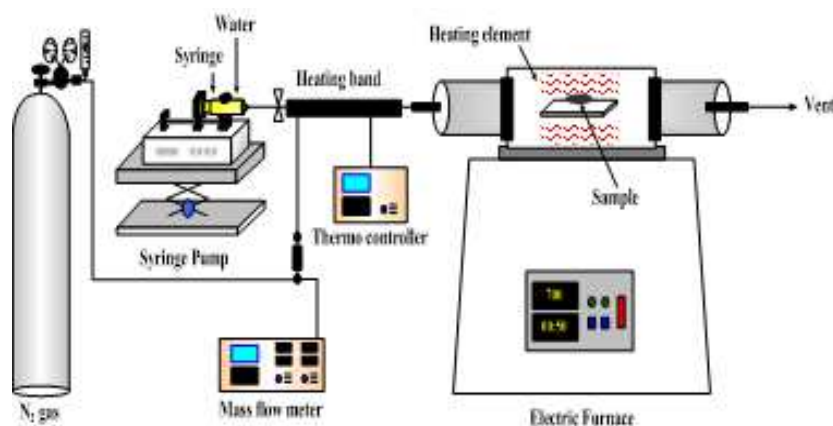


Figure 3.1 Experimental apparatus for conventional carbonization

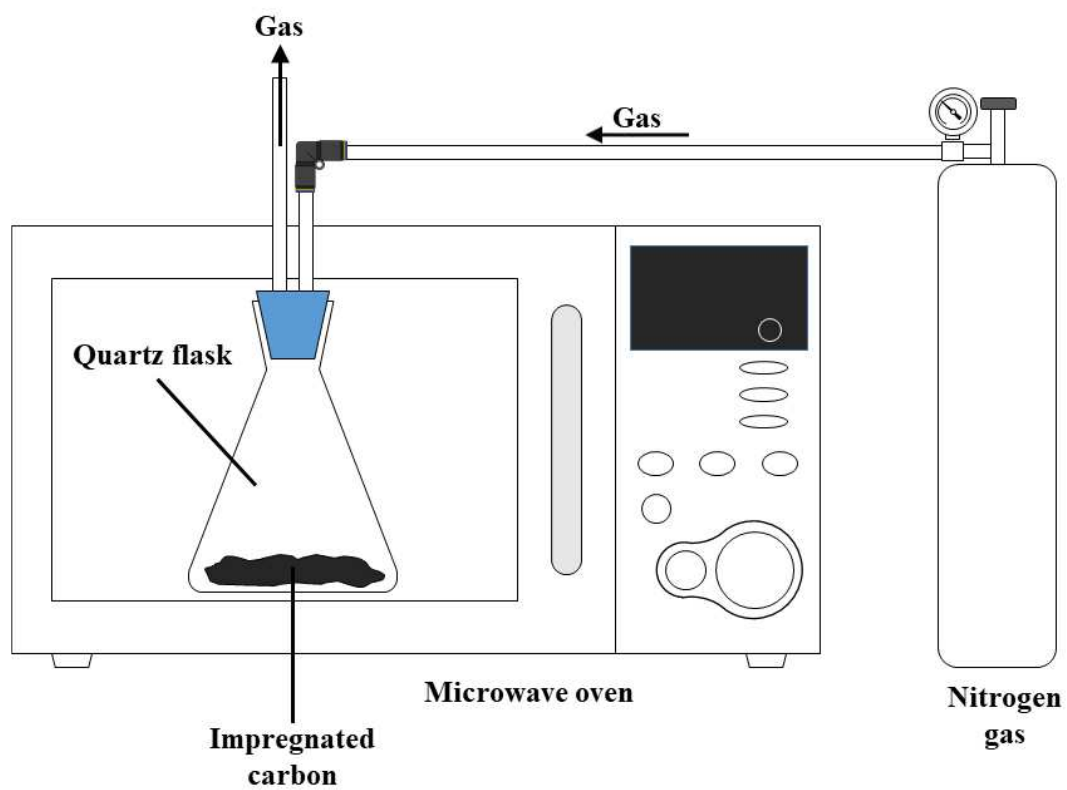


Figure 3.2 Experimental apparatus for microwave activation

Then, derivative thermogravimetric curves (burning profiles) were obtained for the combustion of giant *Miscanthus* and *Chlorella ellipsoidea* biomass. A scanning electron microscope (SEM) was used to observe the surface structure and pore development of carbon samples. The prepared carbon samples were examined on transmission electron microscope (TEM) (Topcon 002B, Topcon Corp. Japan) operating at 200 kV. X-ray diffraction measurements using a Bruker D8 Advance diffractometer through nonmonochromatic Cu K α X-ray at 40 kV and 40 mA were conducted. The surface functional groups of the samples was analyzed by FT-IR spectra using a PHI5700 ESCA FTIR system sung KBr disks prepared by mixing 0.5% of finely ground carbon sample in KBr. Pellet made of pure KBr was used as a reference sample of background measurements. The spectra were recorded from 4000 to 400 cm⁻¹ at a resolution of 4 cm⁻¹. N₂ adsorption-desorption isotherms were obtained using an mirae scientific instruments (nanoPOROSITY, Gwangju, Korea). Prior to measurements, the carbon samples were degassed under vacuum for 3 h. The specific surface area was determined by the Brunauer-Emmet-Teller (BET) method at relative pressure (P/P₀) of 0.05 to 0.25, and the specific surface area of micropores was calculated using t-plots. The average pore size of the sample was evaluated using Barrett-Joyner-Halenda (BJH) desorption method. The micropore volume was calculated by the t-plot and BJH methods. The pH titration was conducted in 100 mL suspension solution containing 1.0 g/L of porous carbon. Nitrogen gas was introduced to remove any dissolved CO₂ before HCl was added to lower solution pH to 3. The concentration of HCl solution was titrated with 0.1M NaOH upto pH 10. The determination of pH_{pzc} was conducted by adjusting the pH of 50 cm³ 0.02 M KCl solution to a value between 1 and 14. After adding carbon samples of 0.4 g, the final solution pH was determined after 24 h under agitation. The pH_{pzc} is determined from the point where pH_{initial} - pH_{final} = 0.

3.3. Adsorption equilibrium kinetics measurements

For the adsorption kinetics experiments, methylene blue adsorption was conducted in adsorber of 500 mL at 25 °C. The initial concentration of methylene blue was set as 10 mg L⁻¹. A small quantity was taken out from the adsorber for different contacting times (5 ~ 180 min). The whole mixture of methylene blue and power activated carbons was separated by filtration. Methylene blue concentration was measured using a UV spectrophotometer at 660 nm. In the adsorption isotherm experiments, a 0.1 g of the carbon samples was add to 250 mL and 5 ~ 20 mg L⁻¹ dye solution and then was contacted for 24 h at 150 rpm in a rotary mechanical shaker at constant temperature (20, 50, 60 °C) to reach equilibrium. The amount of methylene blue of q_t (mg g⁻¹) at time t was calculated by the following equation :

$$q_t = \frac{(C_0 - C_t)}{w} V \quad (\text{Eq. 3.1})$$

where q_t (mg g⁻¹) is amount of solute adsorbed from the solution per g of sorbent at time t (min). C_0 (mg L⁻¹) is the initial concentration, C_t (mg L⁻¹) is the concentration of methylene blue solution at time t , V (mL) is the volume of the aqueous solution, and w (g) is the weight of the adsorbent.

3.4. Electrochemical measurement

3.4.1. Preparation of electrode

The carbon electrode was prepared by the phase inversion method using activated carbon as the active material and polyvinylidene fluoride as the binder. The preparation process is illustrated in **Figure 3.3**. A binder solution was prepared by dissolving 1 g of polyvinylidene fluoride in 25 mL dimethyl acetamide solution with stirring at 80 °C for 4 h. To prepare a carbon electrode, 9 g carbon materials was poured into 25 mL binder

solution to prepare a uniform electrode slurry by paste mixer (PDM-300, Dae Wha Tech). The prepared electrode slurry was cast on graphite sheet using doctor blade to be about 160 to 170 μm in thick, and then dried at 60 $^{\circ}\text{C}$ for 2 h.

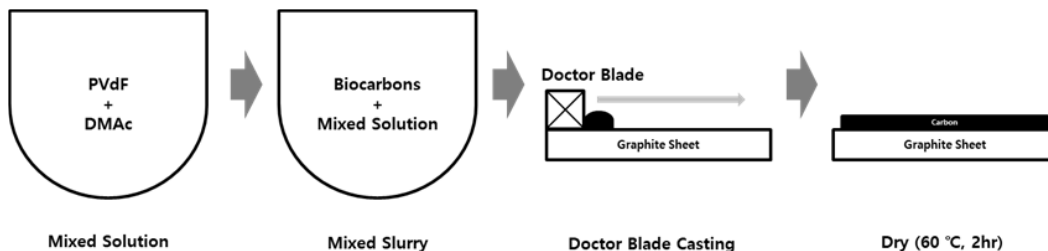


Figure 3.3 Preparation of biocarbon electrodes

The electrochemical performance of the carbon electrode prepared from biocarbons was evaluated by cyclic voltammetry (CV) using an electrochemical workstation (CHI660E, USA) with a three-electrode system. The working electrode, counter electrode, and reference electrode were a platinum wire attached to the biocarbon electrode with a conductive carbon paste (2 – 3 mg), a platinum wire, and an saturated Calomel electrode (SCE), respectively. Cyclic voltammograms were obtained in a potential window of -1.0 to 1.0 V with different scan rates (10 – 200 mV s^{-1}) for assessing the voltammetric capacitance of the carbon electrode and electrolyte solution of 1 M potassium chloride. The specific capacitance was determined from the CV curves from the following relationship:

$$C = \frac{(i_a - i_c)}{v \cdot m} = \frac{\Delta i}{v \cdot m} \quad (\text{Eq. 3.2})$$

where C represents the specific capacitance (F g^{-1}), i_a is anodic current (A) and i_c is cathodic current (A), v is scan rate (V s^{-1}), and m is the mass of the carbon electrode (g). To determine the specific capacitance from the cyclic voltammetry experiments, the measured electrical current is divided by the scan rate (v) and the sample weight of carbon electrodes according to the (Eq. 3.2).

3.5. Dissolved air flotation

3.5.1 Coagulation and Flocculation

Before sedimentation and DAF operation, coagulation of powdered biocarbons was examined on a Jar-Test apparatus using polyaluminium chloride of $\text{AlCl}_3 \cdot 6\text{H}_2\text{O}$ (Junsei Co., Japan) as a coagulant having a gram molecular weight of 241.45. The coagulant was added to the dye solution and was rapidly mixed (140 rpm) for 1 min followed by slow mixing (20 rpm) for 7 min and then allowed to settle for 1 h. The supernatant after the treatment was used to determine the concentration of residual PAC. Zeta potential (Photal Otsuka ELS-8000, Japan) was evaluated to investigate the characteristics of surface charge to obtain further insight in the mechanism of removal. The experimental apparatus for dissolved air flotation is shown in **Figure 3.4**. The experimental conditions for DAF and CGS are listed in **Table 3.2**. The flotation column was made of plexiglass having 10 cm in diameter and the height in 30 cm. Powdered biocarbon particles were suspended initially in the column, then bubbles were supplied in the column from the bottom side of the column. The dissolved air solution was introduced into the flotation column and the particles in the column were removed by the rising bubbles depending on the collision and attachment efficiency. The mean diameter of the bubbles fed into the column was 25 μm . After all the bubbles in the cell reached the top of the column, the solution was withdrawn to evaluate the flotation efficiency. The concentrations of particles were determined using the turbidity meter (HACH 2100P).

Table 3.2 Experimental conditions for CGS and DAF

Step	Items	Values
Rapid mixing	Paddle speed (rpm)	150
	Time (min)	1
Slow mixing	Paddle speed (rpm)	50
	Time (min)	20
CGS	Sedimentation (min)	30
	Recycle ratio (%)	20
DAF	Saturator pressure (kg cm ⁻²)	5

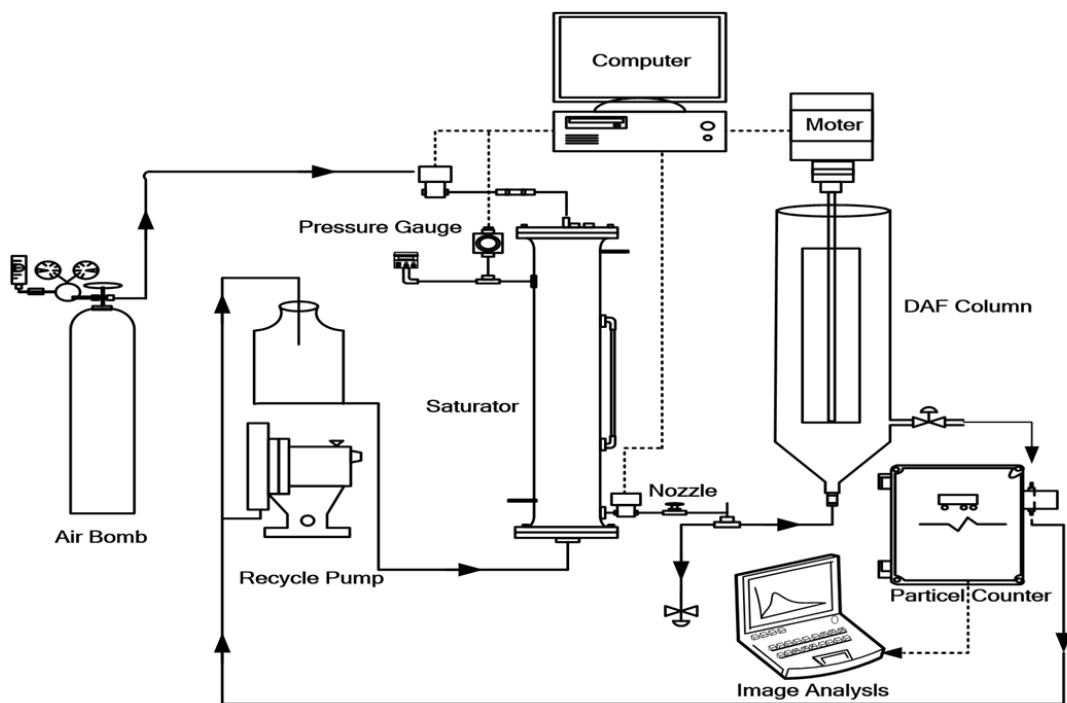


Figure 3.4 Experimental apparatus for dissolved air flotation

Chapter 4

Results and Discussion

4.1 Characterization of porous carbon

Hierarchical porous carbons from giant *Miscanthus* and *Chlorella ellipsoidea* were prepared by carbonization and peroxide-assisted microwave activation. Thermogravimetric curves of the raw giant *Miscanthus* and algae show the suitability of these materials for the preparation of biocarbons. Many factors, including the applied temperature, nature of the precursor, and content of inorganic matter, determine the final physical and chemical properties. **Figure 4.1.** shows the TGA curves for giant *Miscanthus* and algae under a nitrogen atmosphere. The weight loss began at 40 °C and gradually increases up to 350 °C. This is followed by a sudden and sharp increase in weight loss between 250 and 350 °C. Contrary to giant *Miscanthus*, the weight loss of algae was progressed smoothly. The final yields of giant *Miscanthus* and algae at 700 °C under nitrogen were 10 % and 7 %, respectively

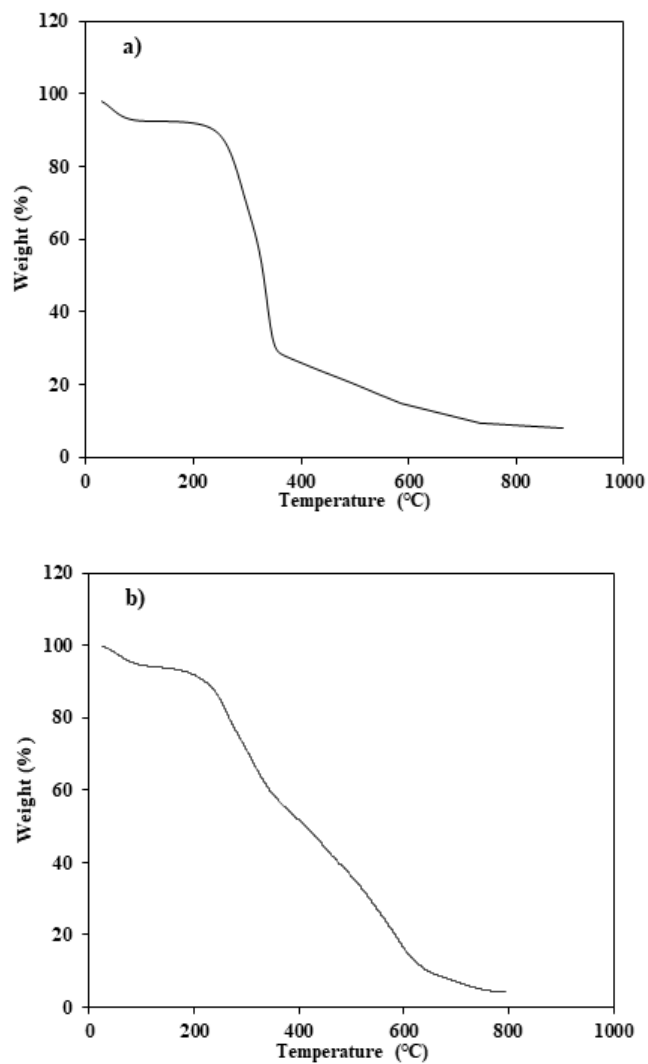


Figure 4.1 TGA result of a) Giant *Miscanthus* b) *Chlorella ellipsoidea*

Figure 4.2 shows the FE-SEM images and EDX of the prepared carbons of giant *Miscanthus* depending on the temperatures. Interestingly, it can be observed that all samples have honeycomb-like structure for raw, carbonization and activation samples. Also, the carbon contents increased from 65.49 % to 87.33 % (**Table 4.1**).

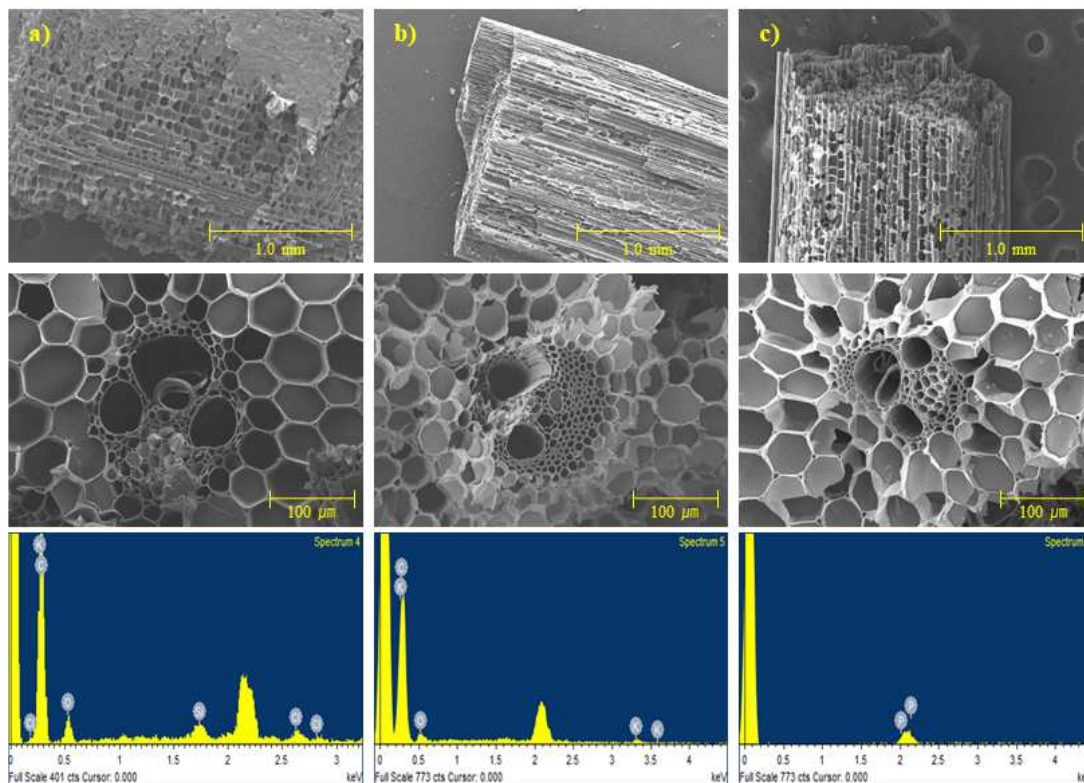


Figure 4.2 SEM images and EDX of Giant *Miscanthus* a) Raw, b) Carbonization, c) Activation

Table 4.1 Elemental analysis for samples of raw, carbonization and activation

	Carbon (%)	Hydrogen (%)	Potassium (%)
Raw	65.49	17.65	16.86
Carbonization	75.84	20.45	1.85
Activation	87.33	12.19	0.47

The carbonized samples were activated using hydrogen peroxide. Prior to activation, the carbonized sample was obtained direct heat treatment at 700 °C under nitrogen atmosphere. The impregnation of H₂O₂ on the biocarbons was carried out as follows. 2 g of biocarbon was put into 30 mL of H₂O₂ solution. The mixtures were stirred using a magnetic stirrer at 200 rpm for different time periods (6 h, 12 h, or 24 h). H₂O₂-impregnated biocarbons were vacuum filtered, and the solids were treatmented in the microwave reactor under microwave power (700 W). The microwave treatment was carried out for 2.5, 5, 7, 10 and 15 min. After the activation, the reactor was cooled to ambient temperature prior to the removal of the activated carbon. As shown in **Figure 4.3**, an example of scanning electron micrographs at different locations and magnifications for porous carbon (MS-0-0) prepared from giant *Miscanthus* without microwave activation and H₂O₂-impregnated MS-12-7.5. Also, **Figure 4.4** shows an typical example of scanning electron micrographs for porous carbon (CH-700) from algae biomass prepared by peroxide-assisted microwave activation (CH-700-H12). H₂O₂-impregnated carbon results in opening up of the micron-sized spots generated during microwave irradiation. In addition, the formation of nanoparticles and nonotube-like structures is observed in some regions on the surface of carbons. These results may come from the fact that the microwave on H₂O₂-impregnated carbons cause the microexplosions in the vicinity of the carbon surface. Thus, the formation of more internal pores of smaller diameter acts as possible adsorption sites.

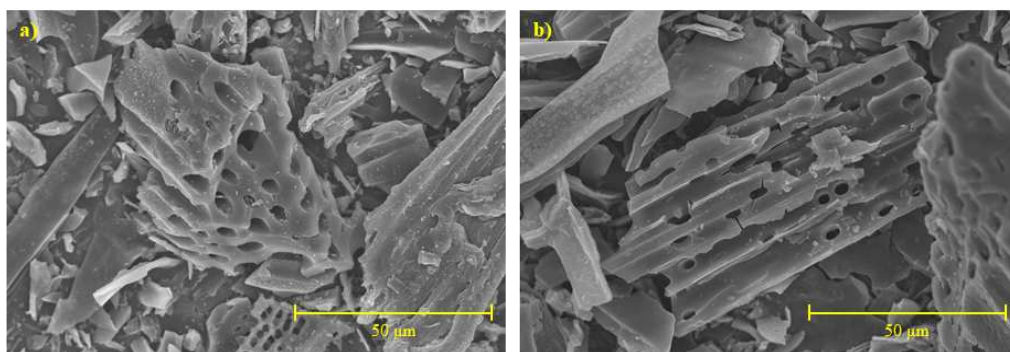


Figure 4.3 SEM images of a) MS-0-0, b) MS-12-7.5

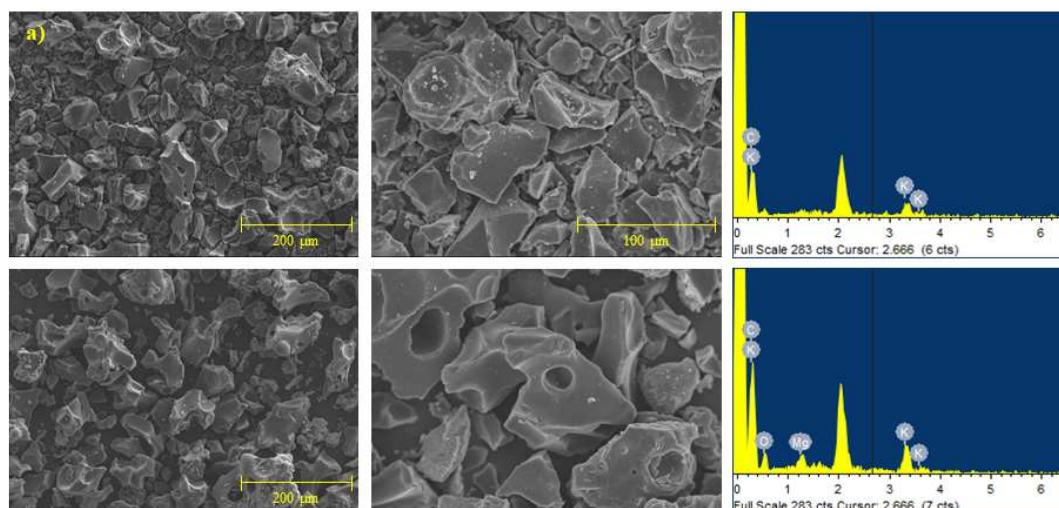


Figure 4.4 SEM image and EDX of a) CH-700, b) CH-700-H12

Table 4.2 Elemental analysis for samples of CH-700 and CH-700-H12

	Carbon (%)	Potassium (%)	Oxygen (%)
CH-700	96.43	3.57	-
CH-700-H12	77.67	3.21	17.71

The particle size distribution of the powdered activated carbon is very important especially when it is applied to adsorption equilibrium and kinetics as well as dissolved air flotation for water and wastewater treatment. **Figure 4.5** shows the particle size distribution of porous carbon (MS-0-0) without microwave activation and H₂O₂-impregnated MS-12-7.5. Also, the average particle size of porous carbon (CH-700) from algae biomass prepared by peroxide-assisted microwave activation (CH-700-H12) was examined. The average particle size of CH-700 was 998 nm (**Figure 4.6**).

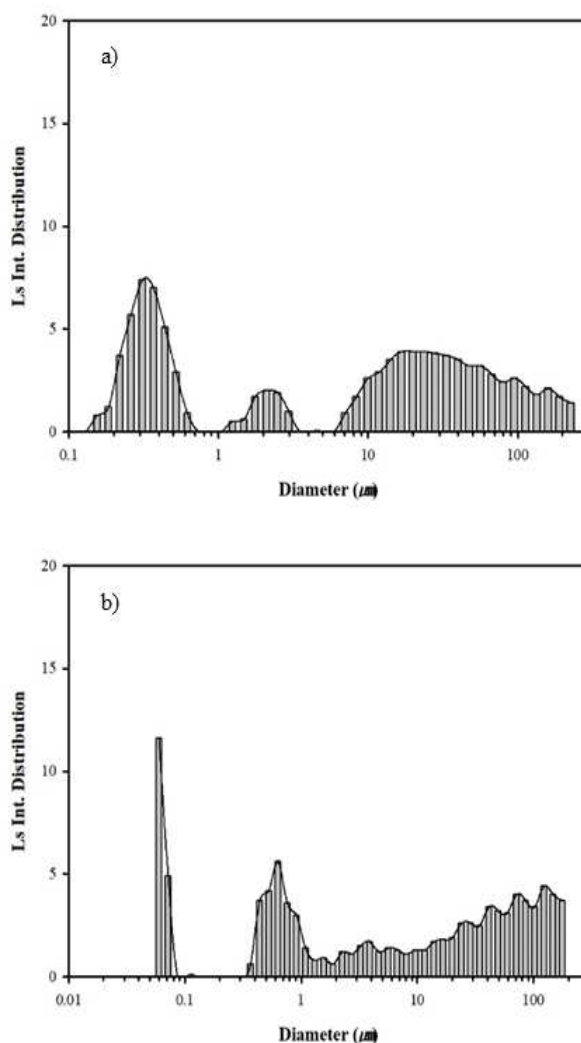


Figure 4.5 Particle size distribution of a) MS-0-0, b) MS-12-7.5

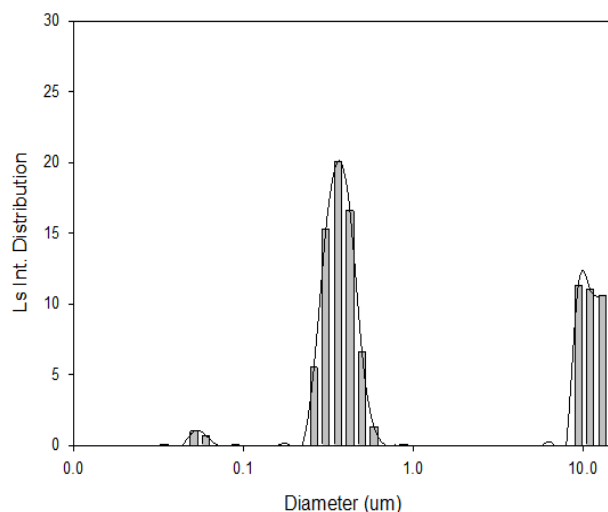


Figure 4.6 Particle size distribution of CH-700

Figure 4.7 shows the XRD patterns of the CH-700 and CH-700-12 samples. Clearly, all samples have two strong and weak diffraction peaks appearing around 25° and 45° corresponding to (002) and (100) planes of amorphous carbon. It confirms that they have a disordered structure. The weak (002) peak indicates low graphitization degree and disordered arrangement of carbon layers. The (100) peak indicates that the presence of honeycomb structure formed by sp^2 hybridized carbons.

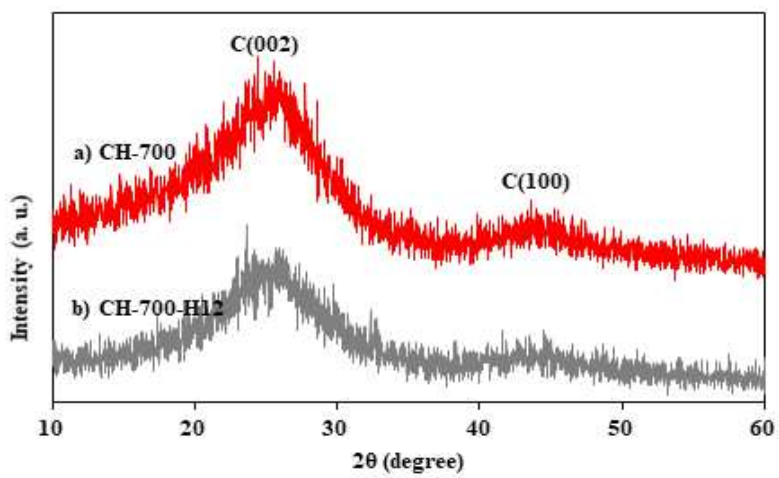


Figure 4.7 XRD patterns of a) CH-700 and b) CH-700-H12

Figures 4.8 show the FT-IR spectra of untreated (MS-0-0, CH-700) and treated carbons (MS-12-7.5, CH-700-H12) indicating strong absorption peaks in the region of 3500~1000 cm^{-1} . In general, these peaks could be attributed to the antisymmetric strengthening vibration of -OH (at 3435 cm^{-1}), -CH₃ and -CH₂ (at 2924 cm^{-1}), C-O (1068 cm^{-1}) and C=O (at 1646 cm^{-1}), respectively. These peaks indicated that the *Miscanthus* contains a lot of cellulose and hemicelluloses. In addition, it can be confirmed that the addition of H₂O₂ increase the content of oxygen functionalities such as carboxylate and hydroxyl groups in the carbon. However, microwave treatment of peroxide impregnated carbon results in the reduction in surface of concentration of these groups, although their significance is present in the FT-IR spectra. This can be attributed to the oxidation of the carbon surface in the presence of H₂O₂ during the microwave treatment.

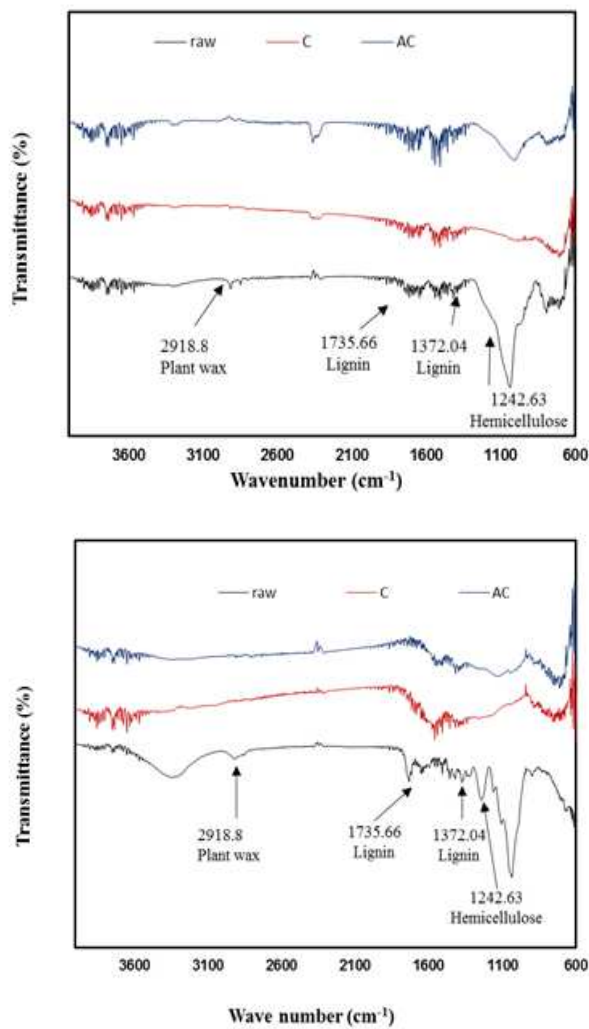


Figure 4.8 FT-IR spectra of untreated and treated carbons (MS-12-7.5, CH-700-H12)

Potentiometric titration was conducted to investigate the origin of surface charge on aqueous biocarbons. Results showed that all biocarbons of CH-900 and CH-900-H12 contained titratable functional groups, indicating that deprotonation of surface functional groups may be responsible for the charge acquisition. It is known that biocarbons contain acidic functional groups of oxygen-containing functionalities of carboxyl and hydroxyl groups that may dissociate at higher pH and result in negatively charged surfaces.

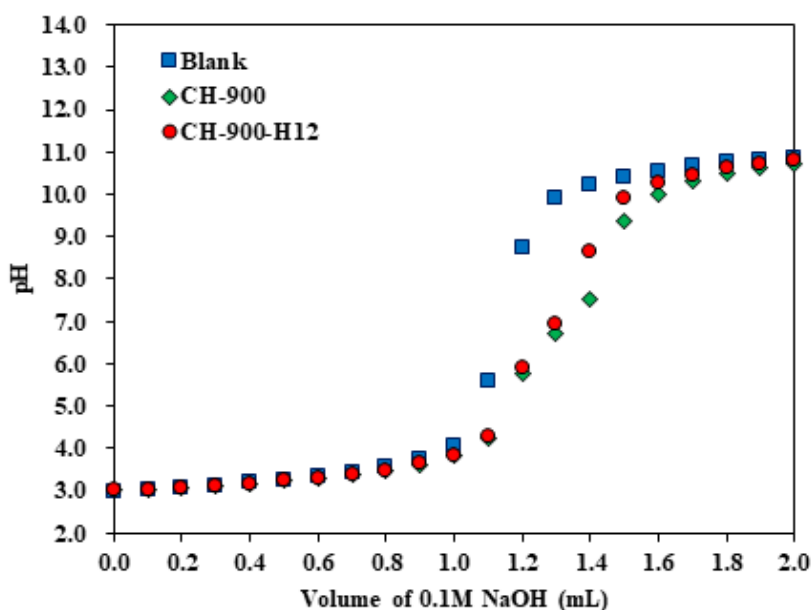


Figure 4.9 Potentiometric titration of biocarbons

Figure 4.10 shows the nitrogen adsorption-desorption isotherms for the two different MS-0-0 and MS-12-7.5. Such isotherms offer plentiful information for understanding the textural nature of the adsorbate-adsorbent system. The nitrogen adsorption-desorption isotherms provide qualitative information on the adsorption mechanism and porous structure of carbonaceous materials. The nitrogen adsorption isotherm analysis of MS-0-0 and modified sample of MS-12-7.5 (**Figure 4.10**). According to the International Union of Pure and Applied Chemistry (IU-PAC) classification, two samples demonstrated that the isotherm resembles type I and type H4 hysteresis isotherms. They showed the same type of hysteresis. This adsorption behavior suggests a combination of microporous-mesoporous structure. This characteristic indicates that absorbents present a mesoporous structure. **Table 4.3** summarizes a comparison of porous structure of activated carbons with and without peroxide treatment. MS-12-7.5 prepared in this study demonstrated a well-developed porous structure with a higher BET surface area of $493 \text{ m}^2 \text{ g}^{-1}$, total pore volume (V_{BJH}) of $0.12 \text{ cm}^3 \text{ g}^{-1}$, and mean pore size of 3.2 nm. Contrary to expectation, the BET surface area of CH-700-H12 was lower than the carbon samples of MS-12-7.5. In addition, wider pore size distribution can be observed (**Figure 4.11**). The surface area, pore volume and pore size are listed in **Table 4.4**.

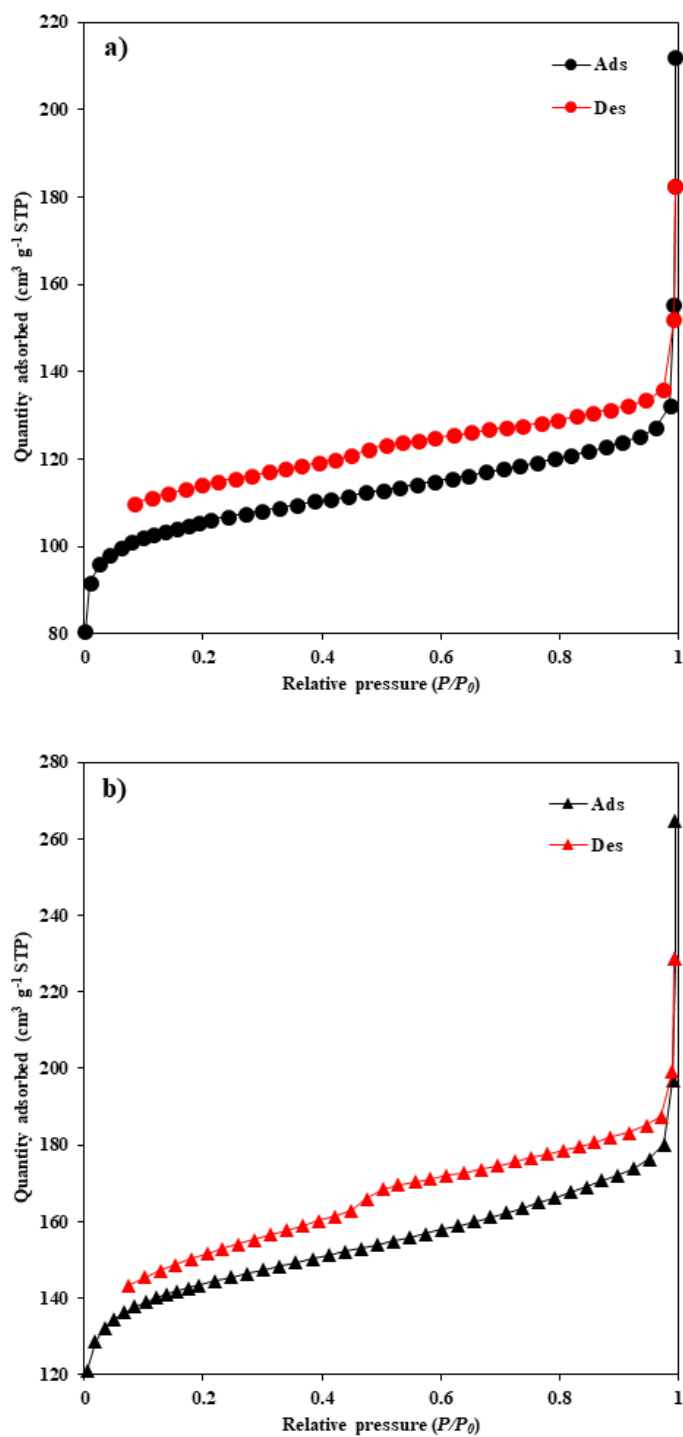


Figure 4.10 Adsorption-desorption isotherms of a) MS-0-0 and b) MS-12-7.5

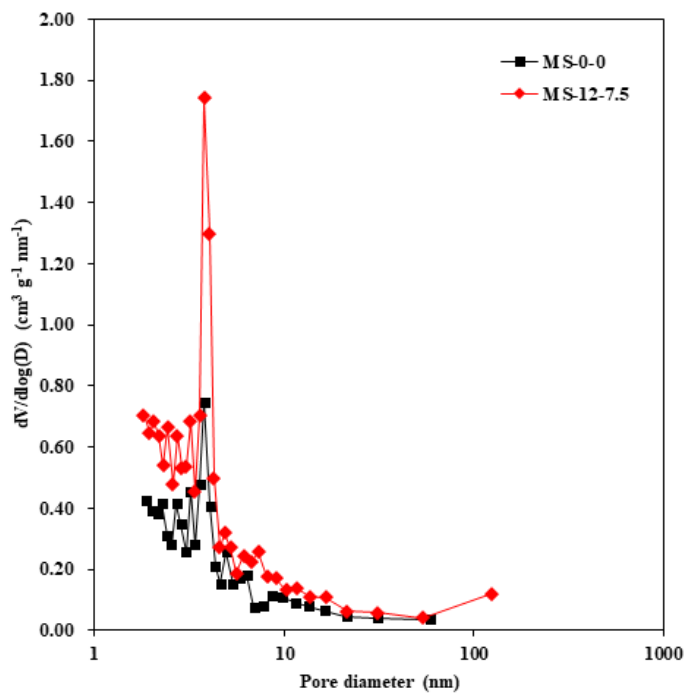


Figure 4.11 Pore size distribution of MS-0-0 and MS-12-7.5

Table 4.3 Textural characteristics of untreated carbon and activated carbon

Sample	Surface area	Pore volume		Pore size	
	(m ² g ⁻¹)	(cm ³ g ⁻¹)		(nm)	
	BET	V _{BJH}	V _{HK}	D _{BJH}	D _{HK}
MS-0-0	360	0.06	0.16	3.2	0.88
MS-12-7.5	493	0.12	0.21	3.2	0.54

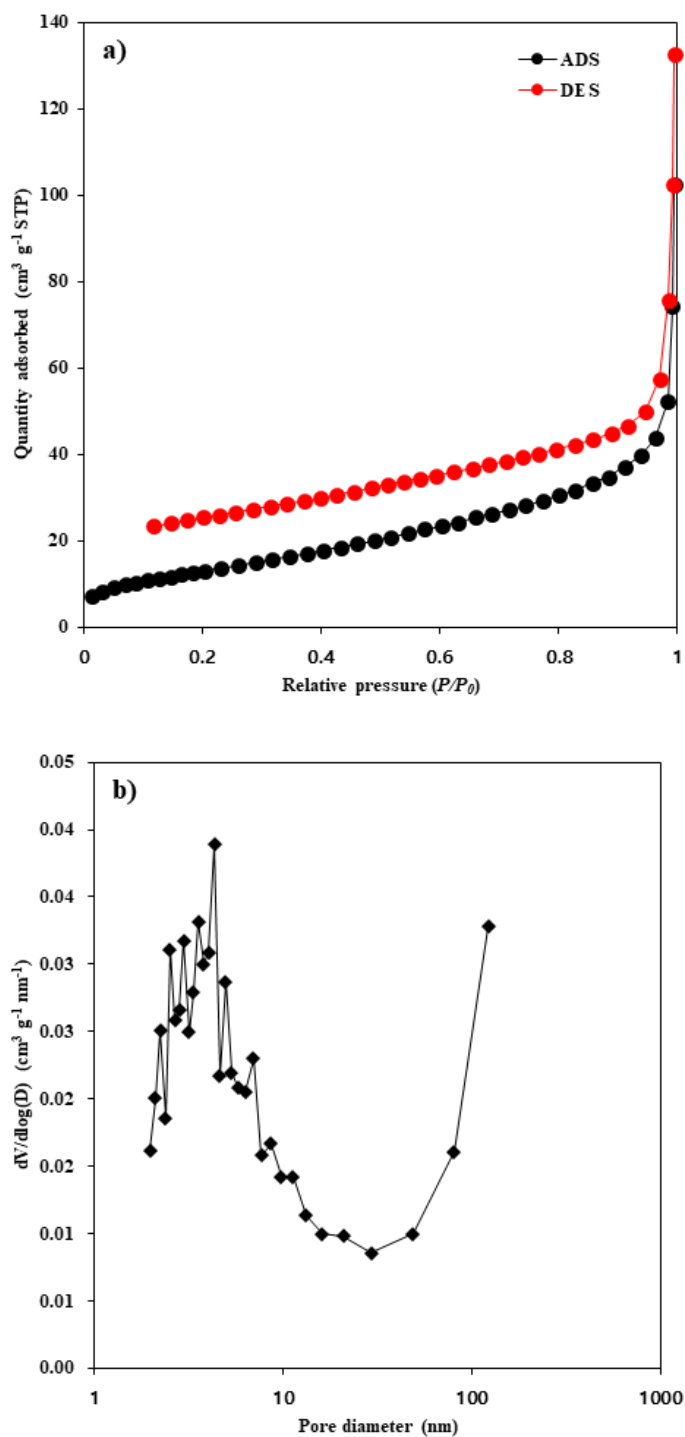


Figure 4.12 Adsorption-desorption isotherms (top) and pore size distribution (bottom) of CH-700

Table 4.4 Textural characteristics of CH-700-H12

Sample	Surface area	Pore volume		Pore size	
	(m ² g ⁻¹)	(cm ³ g ⁻¹)		(nm)	
	BET	V _{BJH}	V _{HK}	D _{BJH}	D _{HK}
CH-700-H12	47.93	0.10	0.02	3.99	1.30

4.2. Adsorption and electrochemical properties

Figure 4.13 shows the adsorption capacity of porous carbon from giant *Miscanthus* biomass depending on H₂O₂ impregnation time (6, 12, 24, 48 h) and microwave radiation time (2.5, 5, 7.5, 10, 12.5, 15 min). The highest adsorption capacity of methylene blue can be observed for MS-12-7.5. On the other hand, **Figure 4.14** shows the adsorption capacity of methylene blue on porous carbon (CH-700) prepared from algae biomass carbons (CH-700-D06, CH-700-H06, CH-700-H12, CH-700-H12) employing peroxide-assisted microwave activation. The maximum capacity of methylene blue on CH-700-H12 was 30 mg g⁻¹.

To understand the rate controlling step in the adsorption of MB on hierarchical porous carbons, the kinetic experimental data were obtained for the carbon samples prepared under different peroxide-assisted microwave activation. The linearized plot of the first and second order kinetic equations are given as follows

First-order-kinetic model:

$$\log(q_e - q_t) = \log q_e - \frac{k_1 t}{2.303} \quad (\text{Eq. 4.1})$$

Second-order-kinetic model:

$$\frac{q_e}{t} = \frac{1}{k_2 q_e^2} + \frac{t}{q_e} \quad (\text{Eq. 4.2})$$

The model parameters of those models were determined from the slope and intercept of the linear plot of Eqs. (4.1) and (4.2). The determined values are listed **Table 4.5**, **Figure 4.15** shows that the pseudo-second-order model fits the experimental kinetic data of a) MS-0-0, (b) MS-12-5, and (c) MS-12-7.5 in 10 mg L⁻¹ MB solution. The solid lines in **Figure 4.16** are the predicted results based on pseudo-second-order kinetic model using the kinetic

parameters (Table 4.5) at different concentration of 10, 20, 50 mg L⁻¹ MB solution. On the other hand, Figure 4.17 shows the adsorption kinetics of methylene blue on untreated carbon and treated carbons a) concentration change over time and b) pseudo-second order kinetic models. Here the solid lines are the predicted results using kinetic parameters listed in Table 4.6. It was found that the pseudo-second order kinetic model can successfully fit the kinetic data of carbons prepared from both giant *Miscanthus* and algae biomass.

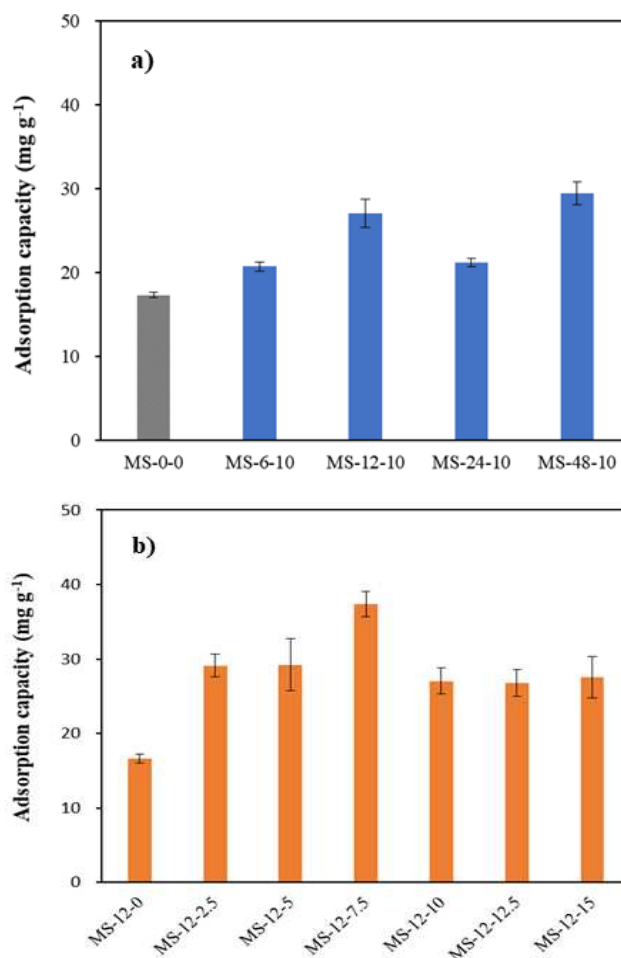


Figure 4.13 Effect of (a) impregnation time and (b) microwave radiation time

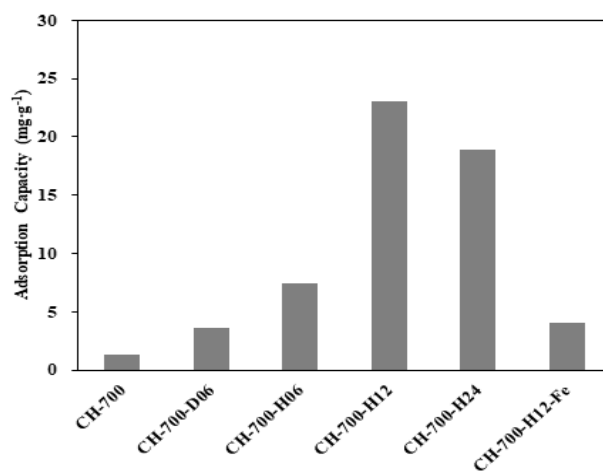


Figure 4.14 Adsorption capacity of methylene blue on algae biomass carbons

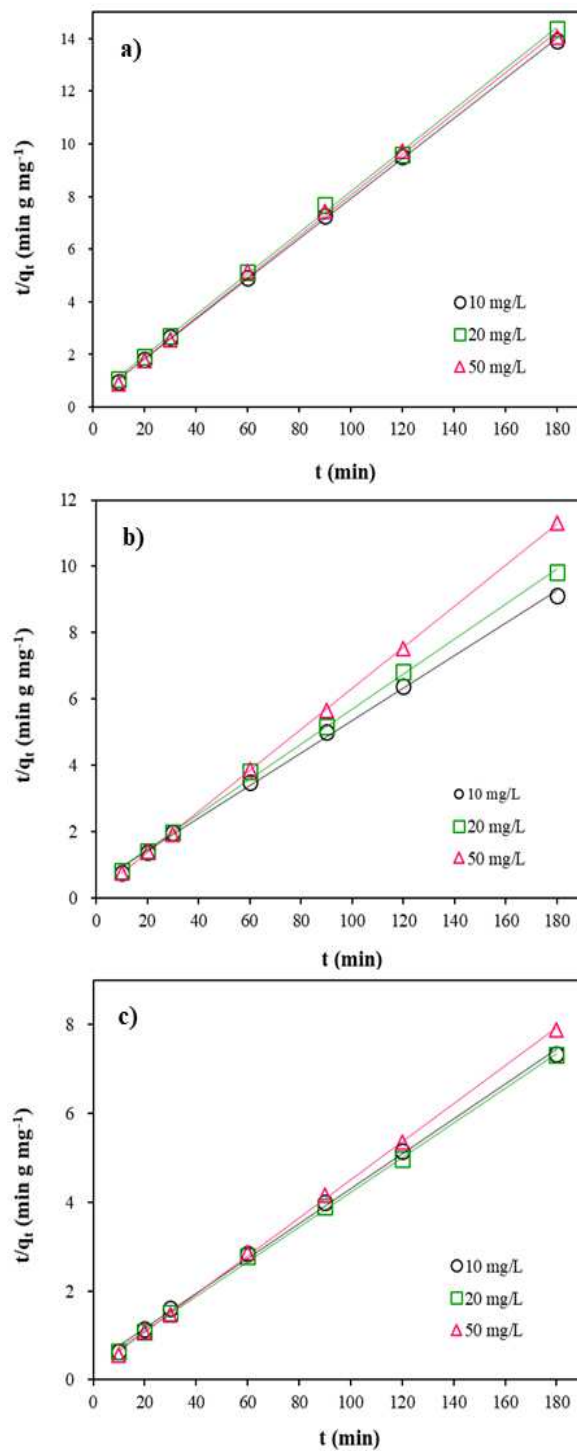


Figure 4.15 Pseudo-second-order plots of a) MS-0-0, b) MS-12-5, c) MS-12-7.5 and comparison of samples in 10 mg L⁻¹ MB solution

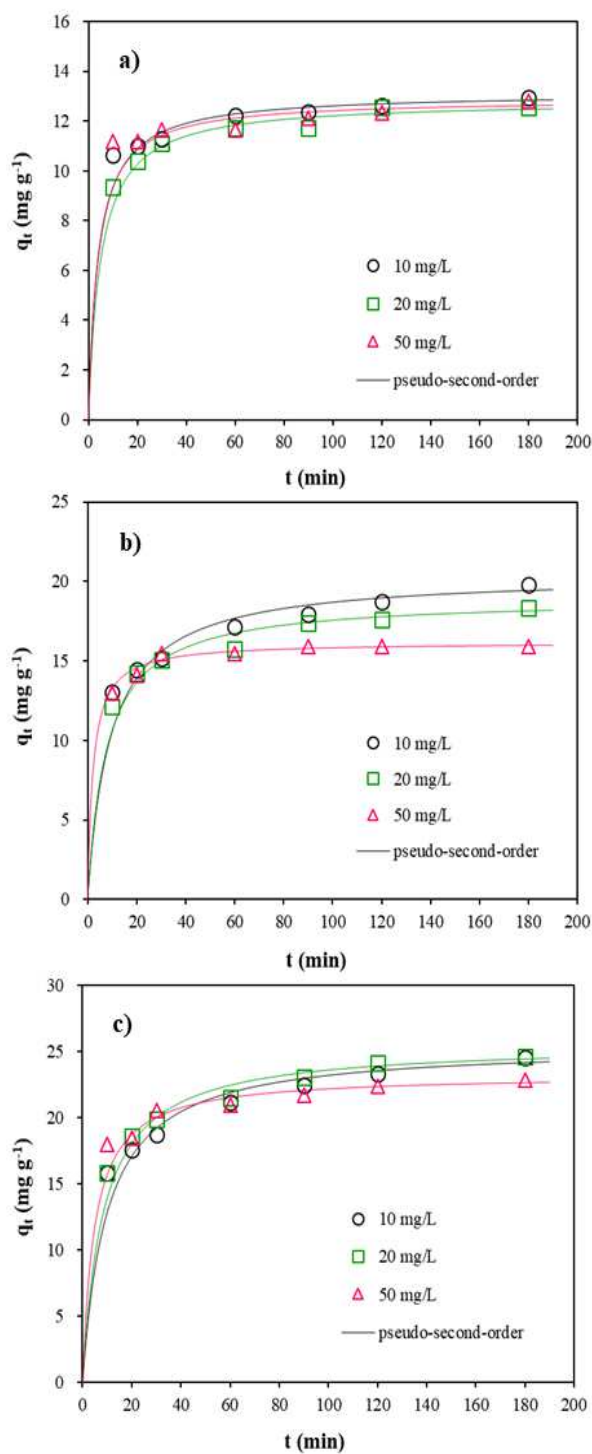


Figure 4.16 Pseudo-second-order kinetic models of a) MS-0-0, b) MS-12-5, c) MS-12.7.5 in different concentration of MB solution

Table 4.5 Adsorption kinetics parameters for giant *Miscanthus* carbons

Adsorbents	Concentration (mg L ⁻¹)	Parameters					
		Pseudo-second-order model			Pseudo-first-order model		
		k_1 (g mg ⁻¹ h ⁻¹)	q_e (mg g ⁻¹)	R^2	k_1 (h ⁻¹)	q_e (mg g ⁻¹)	R^2
MS-0-0	10	1.12	13.1	1.00	1.09	12.9	0.98
	20	0.94	12.8	1.00	0.99	12.5	0.83
	50	1.22	12.9	1.00	0.67	12.8	0.95
MS-12-5	10	0.31	20.4	1.00	1.00	19.8	1.00
	20	0.41	18.9	1.00	1.17	18.3	0.96
	50	1.69	16.2	1.00	2.20	15.9	0.68
MS-12-7.5	10	0.24	25.5	1.00	1.06	24.6	1.00
	20	0.28	25.6	1.00	1.46	24.6	0.97
	50	0.53	23.3	1.00	1.19	22.8	0.96

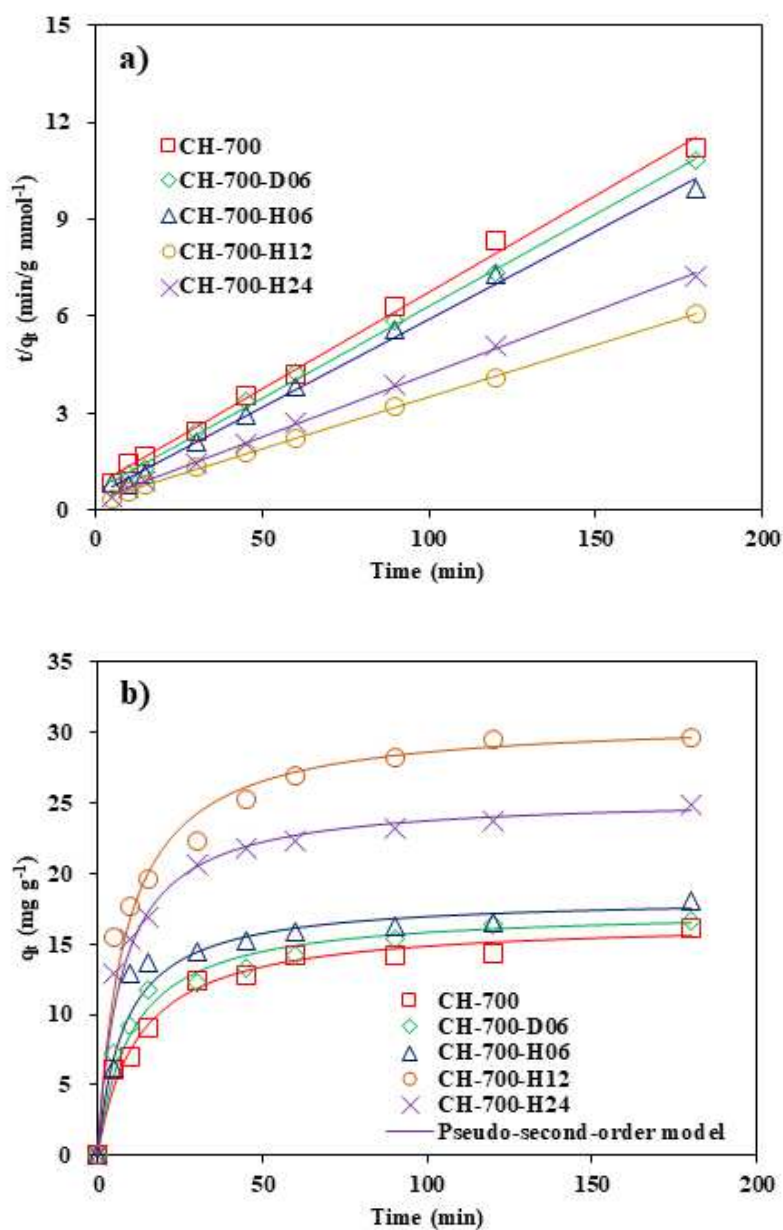


Figure 4.17 Adsorption kinetics of methylene blue on untreated carbon and treated carbons a) concentration change over time, b) pseudo-second order kinetic models

Table 4.6 Adsorption kinetics parameters for algae biomass carbons

Adsorbent	Parameters			
	$k_2(\text{g mol}^{-1}\text{min}^{-1})$	$q_e(\text{mmol g}^{-1})$	$h(\text{mmol g}^{-1}\text{min}^{-1})$	R^2
CH-700	0.0048	16.67	1.35	0.99
CH-700-D06	0.0055	17.46	1.68	0.99
CH-700-H06	0.0066	18.33	2.23	0.99
CH-700-H12	0.0038	31.04	3.67	0.99
CH-700-H24	0.0053	25.55	3.47	0.99

Adsorption equilibrium isotherm data is the most effective for analyzing the adsorption process. Adsorption characteristics of methylene blue on biocarbon samples were evaluated on the basis of adsorption equilibrium studies. The adsorption isotherms of methylene blue were obtained for the carbon samples prepared under different peroxide-assisted microwave activation. Among the well-known isotherm models including the Langmuir, Freundlich, Sips, and Dubinin-Radushkevich equations, the Langmuir and Freundlich isotherm models are generally employed for the adsorption on monolayer surface coverage and multiple surface layer, respectively. The isotherm parameters of Langmuir and Freundlich equations are evaluated using the linear regression methods using Eq. 4.3 and Eq. 4.4. The linearized equations of Langmuir and Freundlich isotherms are given as follows.

Langmuir equation:

$$\frac{1}{q_e} = \frac{1}{q_m} + \frac{1}{q_m b} \frac{1}{C_e} \quad (\text{Eq. 4.3})$$

Freundlich equation:

$$\ln q_e = \ln k + \frac{1}{n} \ln C_e \quad (\text{Eq. 4.4})$$

Figure 4.18 shows the adsorption isotherms of MS-12-7.5 at different temperatures (25, 35, 45 °C). On the other hand, the thermodynamic parameters (ΔH^0 and ΔS^0) for the adsorption process of MB on MS-12-7.5 were determined from the linear plot of $\ln K_d$ vs. $\frac{1}{T}$ from the Eq. 2.12 (**Figure 4.19**). The determined thermodynamic parameters are listed in **Table 4.8**. Compared to MS-12-7.5, the adsorption isotherm of methylene blue on CH-700-H12 was highly dependant on temperatures of 30 to 60 °C (**Figure 4.20**). The solid lines in **Figure 4.18** and **Figure 4.19** are the predicted results, based on the Langmuir and Freundlich isotherm parameters (**Table 4.7** and **Table 4.9**). The Langmuir, Freundlich and Dubinin-Radushkevich models fit the experimental data of MS-12-7.5 and CH-700-H12. It has been known that the Langmuir isotherm describes the monolayer

surface coverage on the active sites of the adsorbents, while the Freundlich isotherm is used to describe the physical adsorption over multiple surface layer. The determined values of Dubinin-Radushkevich isotherm of q_m (mg g⁻¹) are 26.8, 33.8, 36.1 for 25, 35, 45 °C and those of K_{DR} (mol² J⁻²) are 2.90×10^{-3} , 3.62×10^{-3} , 6.16×10^{-3} , respectively.

The Gibbs free energy describes the degree of spontaneity of the sorption process. ΔH^0 and ΔS^0 were estimated from the slope and intercept of a plot of $\ln K_d$ against $1/T$ (**Figure 4.19** and **Figure 4.21**). When temperature was increased from 25 to 45 °C for giant *Miscanthus* carbon and from 30 to 60 °C for algae biocarbon, the magnitude of free energy change moved to a high negative value suggesting that the adsorption was energetically favourable, rapid and spontaneous. The positive value of adsorption heat (11.42 and 29.93 kJ mol⁻¹) confirmed the endothermic nature of adsorption process and the positive value of standard entropy changes suggested randomness increase at the adsorbent-solute interface during the adsorption process.

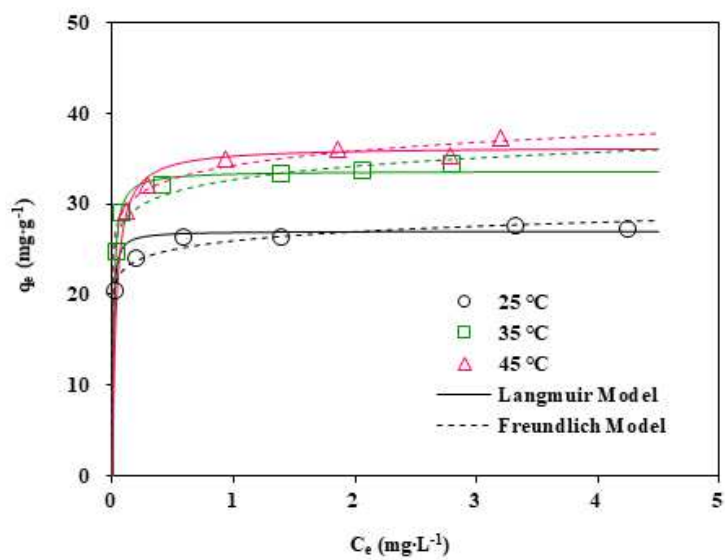


Figure 4.18 Adsorption isotherms of MS-12-7.5 at different temperatures

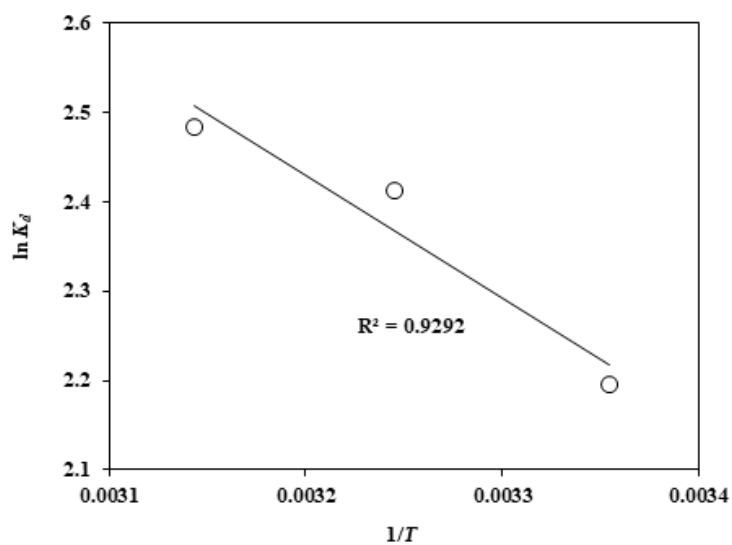


Figure 4.19 A plot of $\ln K_d$ vs. $\frac{1}{T}$ for the adsorption process of MB on MS-12-7.5

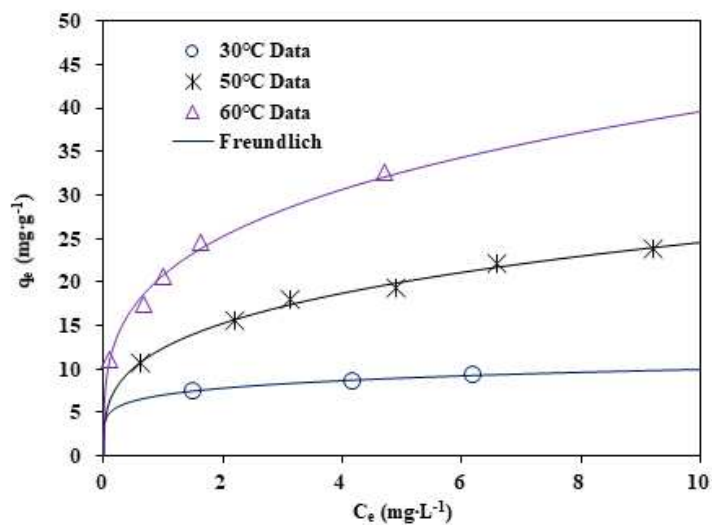


Figure 4.20 Adsorption Isotherm of Methylene blue on CH-700-H12 depending on temperatures

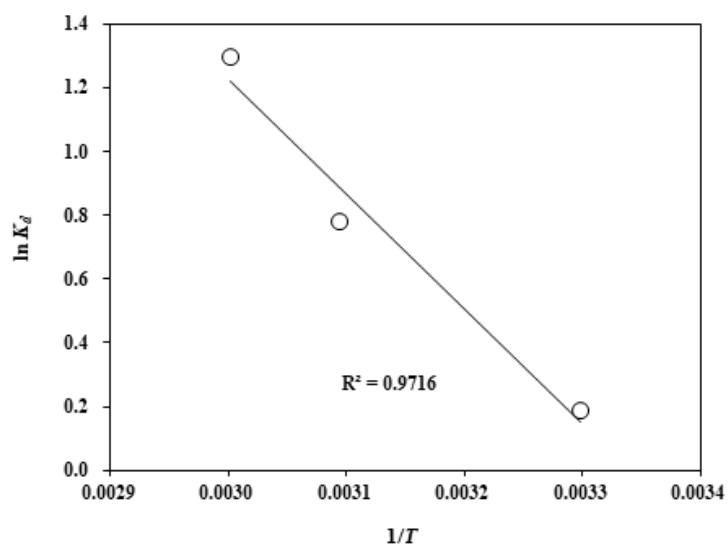


Figure 4.21 A plot of $\ln K_d$ vs. $\frac{1}{T}$ for the adsorption process of MB on CH-700-H12

Table 4.7 Adsorption isotherm parameters for *Miscanthus Sacchariflorus* Carbon

Adsorbents	Temperature (°C)	Parameters			
		Langmuir		Freundlich	
		q_m	b	k	n
MS-12-7.5	25	27.0	161.8	25.9	18.3
	35	33.6	95.4	32.7	15.7
	45	36.3	34.1	34.3	15.5

Table 4.8 Thermodynamic parameters for the adsorption of MB onto MS-12-7.5

ΔG^0 (kJ mol ⁻¹)			ΔH^0 (kJ mol ⁻¹)	ΔS^0 (kJ mol ⁻¹ K ⁻¹)
25°C	35°C	45°C		
-5.44	-6.18	-6.57	11.42	0.0567

Table 4.9 Adsorption isotherm parameters for CH-700-H12

Adsorbents	Temperature (°C)	Parameters			
		Langmuir		Freundlich	
		q_m	b	k	n
CH-700-H12	30	10.4	0.6	7.0	6.6
	50	23.8	0.8	12.4	3.4
	60	25.1	0.1	20.8	3.6

Table 4.10 Thermodynamic parameters for the adsorption of MB onto CH-700-H12

ΔG^0 (kJ mol ⁻¹)			ΔH^0 (kJ mol ⁻¹)	ΔS^0 (kJ mol ⁻¹ K ⁻¹)
30°C	50°C	60°C		
-0.47	-2.10	-3.59	29.93	0.10

Electrochemical capacitor is a promising energy storage device providing usually high power density and longer cycle life with lower energy density. For example, the electrical double layer capacitor is an important properties of electrochemical storage device. It has been known that the electrical energy is accumulated in an electrical double layer through the separation and the pure electrostatic attraction of charge at the interface between the charged surface on an electrode and ionically conductive electrolyte. A lot of materials have been tried as electrochemical double-layer capacitors and the application is still limited due to the low energy density. Recently, many works on developing and modifying carbon materials by control of the pore size distribution and making electroactive metallic particles or electrical conducting polymers have been investigated to enhance the energy density of capacitor. Many types of carbon materials as a form of powder, fiber, paper (fabric or web), carbon nanotubes and the related nanocomposites have been received much attention as candidates for capacitor electrodes. In especial, activated carbon is a key candidate for the storage of energy because of its unique surface properties for electrochemical purposes.

It has been known that the activated carbons with high surface area generally has high capacitance. However, a non-linear relationship between the surface area and specific capacitance has been observed. The carbon electrode performance is largely affected by other parameters including pore geometry, pore size, pore size distribution surface functional groups, and size of the electrolyte ions. Widespread application of carbon electrodes may require abundant renewable materials with easy availability and low cost. In a sense, it is urgent to develop the high-performance carbon electrode materials from abundant renewable natural resources. Many naturally occurring materials such as coconut, bamboo, wood, pine cone etc., have been tried as possible precursors for manufacturing activated carbon. Also, our group has recently reported a novel carbon materials prepared from corn grain, *Ceiba pentandra* (L.) Baertn. (kapok), *Pleuropterus multiflorus* TURCZ. (Hasuo) and brewery yeast.

Cyclic voltammetry is an electrochemical technique to measure the current for the applied voltage from an electrochemical cell. Cyclic voltammetry is performed by cycling the potential of a working electrode, and measuring the resulting current. The direction of the

potential is reversed at the end of each scan in cyclic voltammetry. Current increases as the potential reached the reduction potential of the analyte. Likewise, current decreases as the analyte is depleted in the redox reaction.

Cyclic voltammetric measurements were conducted over the potential range of -1.0 to 1.0 V at different scan rates of 10, 20, 50, 100, 150, 200 mV s⁻¹. **Figure 4.22** shows the typical cyclic voltammetric curves of MS-12-7.5 electrode at different scan rates of 10, 20, 50, 100 mV s⁻¹. Similarly, cyclic voltammetric curves are shown in **Figure 4.23** for CH-700-H12 electrode at different scan rates of 50, 100, 150 and 200 mV s⁻¹. Symmetric AC electrodes were characterized by cyclic voltammetry to observe their profile differences and to determine the voltage window for charge/discharge cycling of MS-12-7.5 and CH700-H12. The determined capacitances are in the range of 29.2 to 69.3 F g⁻¹ for MS-12-7.5 and 3.10 to 4.00 F g⁻¹ for CH-700-H12 as listed in Table 4.7 and Table 4.8. **Figure 4.22** and **Figure 4.23** show the cyclic voltammetric curves with quasi rectangular shape from -1.0 to 1.0 V.

The cyclic voltammetry can be applied to kinetic equations to gain further information about the electron transfer occurring at the working electrode. The oxidation and reduction peak potentials give details on the reversibility of the reaction. The ideal peak separation for a reversible redox couple is independent of scan rate and can be applied to calculate the number of electrons (n) transferred in the reaction.

$$\Delta E_p = E_{pa} - E_{pc} = \frac{57}{n} mV \quad (\text{Eq. 4.5})$$

The Randles Sevcik Equation utilizes the current response (i_p) of an electrochemical redox reaction at various scan rates to analyse an electrochemical process. In this work particularly, the Randles Sevcik equation (Eq. 4.6) has been used current and scan rate from cyclic voltammogram. The scan rate was changed from 10 to 200 mV s⁻¹ and the peak currents were recorded. A plot of the square root of the scan rate was generated as a function of the peak current and a linear relationship was obtained (Figure 4.22 and 4.23).

The Randles-Sevcik equation was applied to evaluate the diffusion coefficient, D , of a particular analyte at a activated carbon electrode, based on Eq. 4.6.

The Randles-Sevcik equation is:

$$i_p = 0.4463nFA C_0 \left(\frac{nFvD}{RT} \right)^{1/2} = \left[0.4463nFA C_0 \left(\frac{nFD}{RT} \right)^{1/2} \right] v^{1/2} \quad (\text{Eq. 4.6})$$

where i_p is peak current (A), n is number of electrons, A is electrode surface area (cm^2), C_0 is analyte concentration (mol cm^{-3}), v is scan rate (V s^{-1}), D is diffusion coefficient ($\text{cm}^2 \text{s}^{-1}$), F is Faraday's constant (96485 C mol^{-1}), R is gas constant ($8.314 \text{ J K}^{-1} \text{mol}^{-1}$), and T is temperature (K). Plotting i_p vs $v^{1/2}$ as suggested yields the following graph for the data recorded at 1 M NaCl electrolyte concentration:

Figure 4.22 and 4.23 show the plot of the peak current as a function of the square root of the scan rate for the data set at 1 M NaCl electrolyte concentration. Both the anodic and cathodic traces were used for this graph. The diffusion coefficient D from the theoretical value of the slope is as follows:

$$\text{slope} = \left[0.4463nFA C_0 \left(\frac{nFD}{RT} \right)^{1/2} \right] \quad (\text{Eq. 4.8})$$

$$D = \left(\frac{\text{slope}}{0.4463nFA C_0} \right)^2 \frac{RT}{nF} \quad (\text{Eq. 4.9})$$

The determined values of a cathodic diffusion coefficient is $2.67 \times 10^{-7} \text{ cm}^2 \text{s}^{-1}$ and anodic diffusion coefficient of $6.68 \times 10^{-7} \text{ cm}^2 \text{s}^{-1}$ for MS-12-7.5 electrode in the experimental conditions. Likewise, the determined diffusion coefficients from cathodic and anodic data of CH-700-H12 are $4.20 \times 10^{-7} \text{ cm}^2 \text{s}^{-1}$ and $6.82 \times 10^{-7} \text{ cm}^2 \text{s}^{-1}$.

Table 4.11 Capacitance of MS-12-7 for different scan rate

MS-12-7.5	Scan rate (mV s^{-1})			
	10	20	50	100
Capacitance (F g^{-1})	65.3	52.8	40.6	29.2

Table 4.12 Capacitance of CH-700-H12 for different scan rate

CH-700-H12	Scan rate (mV s^{-1})			
	50	100	150	200
Capacitance (F g^{-1})	3.90	4.00	3.50	3.10

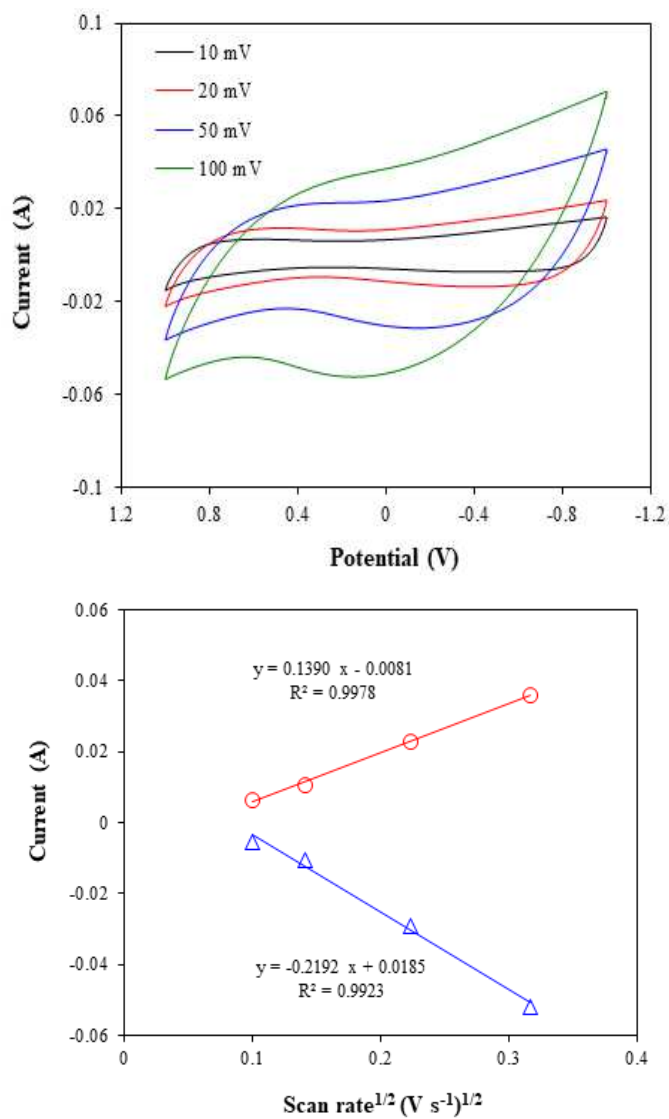


Figure 4.22 CV curves (top) of MS-12-7.5 electrode at different scan rates of 10, 20, 50, 100 mV s⁻¹ and the plot of the peak current as a function of the square root of the scan rate (bottom)

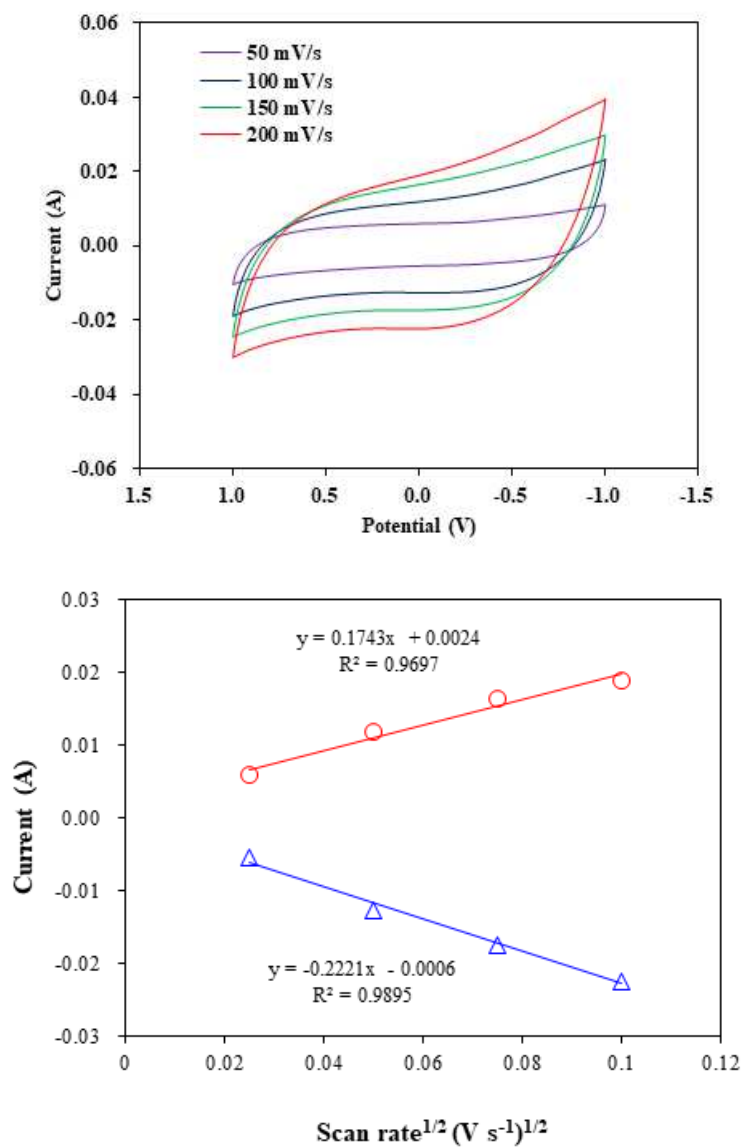
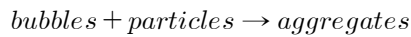


Figure 4.23 CV curves of CH-700-H12 electrode at different scan rates of 50, 100, 150 and 200 mV s^{-1} and the plot of the peak current as a function of the square root of the scan rate (bottom)

The Four Major Rivers (i.e., Han, Geum, Nakdong and Yeongsan) Restoration Project in South Korea stimulate the algae bloom seriously. The source waters in reservoirs generally contain algal particles with low density because of eutrophication of stagnant water basins when nutrients (i.e., nitrogen and phosphorus) from external non-point sources of pollution and internal sediments are released into the water. Algal bloom is an issue that occurs every year despite efforts to solve green algae problems. Algal bloom is caused by the eutrophication. Algae play a key role in the ecosystem as primary producers; however, they can grow in large quantities in water bodies and cause environmental problems such as increasing turbidity, odor generation, water quality deterioration, and degeneration of the ecosystem of the water body and surrounding environment; the last problem is a result of algae depleting the oxygen in the water body and generating sediments when they die [86].

Numerous techniques based on various physical, chemical, and biological principles have been developed to prevent and remove green algae. Among these techniques, the bubble flotation (BF) process (particularly, dissolved air flotation) has been considered the best technique to prevent and remove algae [82]. In DAF process, bubbles and particles interact to form aggregates (or float solids) by considering either reversible 2nd order reaction or 1st order reaction [86].



When considering the number of particles as n_p , the number of bubbles as n_b , and the kinetic constant or rate constant as k_c , the kinetic rates of the 2nd order reaction and 1st order reaction are as follows:

$$\frac{dn_p}{dt} = -k_c n_b n_p = -k'_c n_p \quad (\text{Eq. 4.6})$$

The rate constant is given by

$$k'_c = n_b k_c = n_b (\alpha_{pb} \eta_T A_b U_{pb} n_b) = \frac{3}{2} \frac{\alpha_{pb} \eta_T \phi_b U_{pb}}{d_b} \quad (\text{Eq. 4.7})$$

The input parameters and variables for particle, bubble and water, are described in detail by Kim and Kwak [86].

The dimensionless particle transport or collision coefficient as follows [87]:

$$\eta_T = \eta_D + \eta_I + \eta_S + \eta_{\infty} \quad (\text{Eq. 4.8})$$

The contact efficiency or filtration efficiency (X) is derived from the kinetic rate of the reversible 1st order reaction at steady state. It describes the formation of the bubble—particle aggregate or removal of particles, as expressed in Eq (4.6), where t is the contact time and k'_c is the bubble flotation rate constant depending on the collision coefficient (η_T), attachment coefficient (α_{pb}), bubble diameter (D_b), bubble volume concentration (ϕ_b), approaching velocity between the bubble and the particle (U_{pb}), bubble surface area (A_b), gravitation acceleration (g), and viscosity coefficient (μ), as expressed in Eq (4.7). To determine the rate constant, the collision coefficient (η_T) and the attachment coefficient (α_{pb}) are required based on the trajectory analysis as described in theory section of Eqs. 2.20~2.26. The electrostatic forces acting between particles and air bubbles can be calculated from their ζ -potentials.

Figures 4.24 shows the simulation results using model parameters listed in **Table 4.13** The total collision coefficient or dimensionless particle transport coefficient (η_T) was obtained in various particle diameter ranges. As a result, the smaller the particles, the smaller the bubbles collided to obtain the higher values of particle transport coefficient (η_T). On the other hand, the maximum value for the optimal bubble size existed for every particle. Also, the maximum α_{pb} is obtained when the size of each particle meets the proper bubble size.

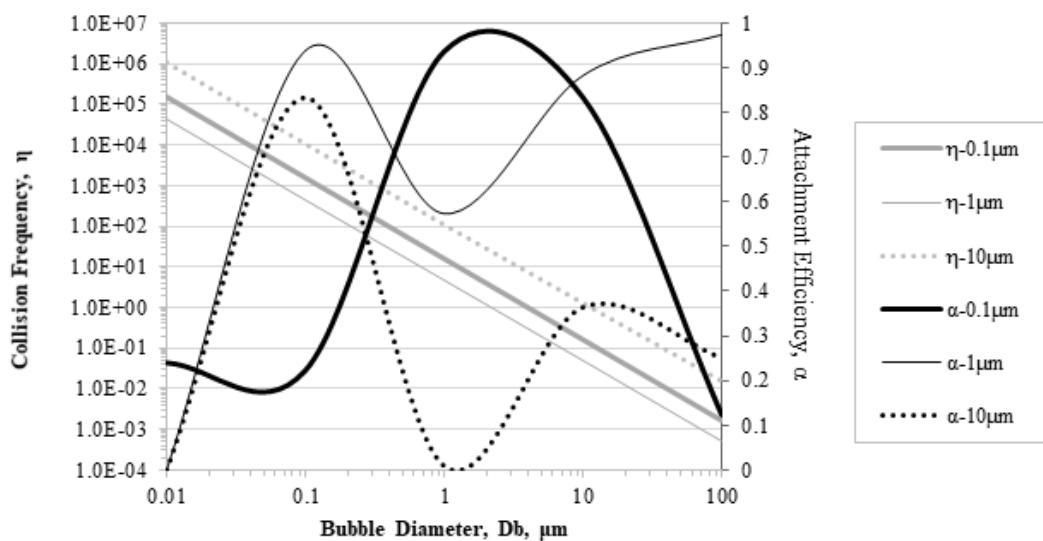


Figure 4.24 Collision frequency and attachment efficiency as functions of bubble and particles size

Stream functions predict the probability of bubble-particle collision over a range of bubble sizes in flotation processes. The stream functions are also applied to predict the probability of adhesion through induction time measurements. Then, the power relationship between flotation rate constant and bubble size is known from these probability functions. It has been known that the flotation rate constants determined experimentally are in good agreements with those predicted from the interceptional collision model. However, the agreement is very limited only when the cell was operated under a relatively quiescent condition. The rate constants obtained using smaller bubbles are decreased, while those obtained using larger bubbles are increased under more turbulent conditions. **Figure 4.25** describes Physical constant for the calculation of electrostatic interaction (V_E), van der Waals dispersion interaction (V_D) and hydrophobic interaction (V_H). When particles and bubbles are oppositely charged, they can be attracted with each other and form bubble-particle aggregates. The van der Waals dispersion forces are repulsive in bubble-particle interactions. The classical DLVO theory (Derjaguin-Landau-Verwey-Overbeek) considers only the electrostatic and dispersion forces. The free energy of bubble-particle interaction (V_T) can be calculated using the extended DLVO theory including electrostatic interaction (V_E), van der Waals dispersion interaction(V_D) and hydrophobic interaction (V_H) (**Figure 4.26**). It can be seen that V_D contributes relatively little to V_T under the experimental conditions listed in **Table 4.13**. Both the electrostatic and dispersion energies are repulsive, while the hydrophobic interaction is the only driving force for air bubble and particle.

Many researchers have studied for the determination of the Hamaker constant and hydrophobic constant to evaluate the electrostatic and hydrophobic interactions [89-107]. Recently, Hen and Huang reported the aggregation kinetics of nanosized activated carbons in aquatic environments [100]. The external surface properties of interacting bodies and the intervening medium are the major parametes to affect the Hamaker constants which provide a tool for evaluating the relative strength of van der Waals attractive interactions. The currently available Hamaker constant data for activated carbons, however, were either estimated from suffogate materials (e.g., carbon fibers, $5.2\sim6.2\times10^{-20} J$) using the contact angle method or calculated from adsorption data ($5.0\sim7.8\times10^{-20} J$) [101-102]. Figure 4.24

shows the flotation efficiency (top), PAC concentration change (middle) and aggregation concentration change (bottom).

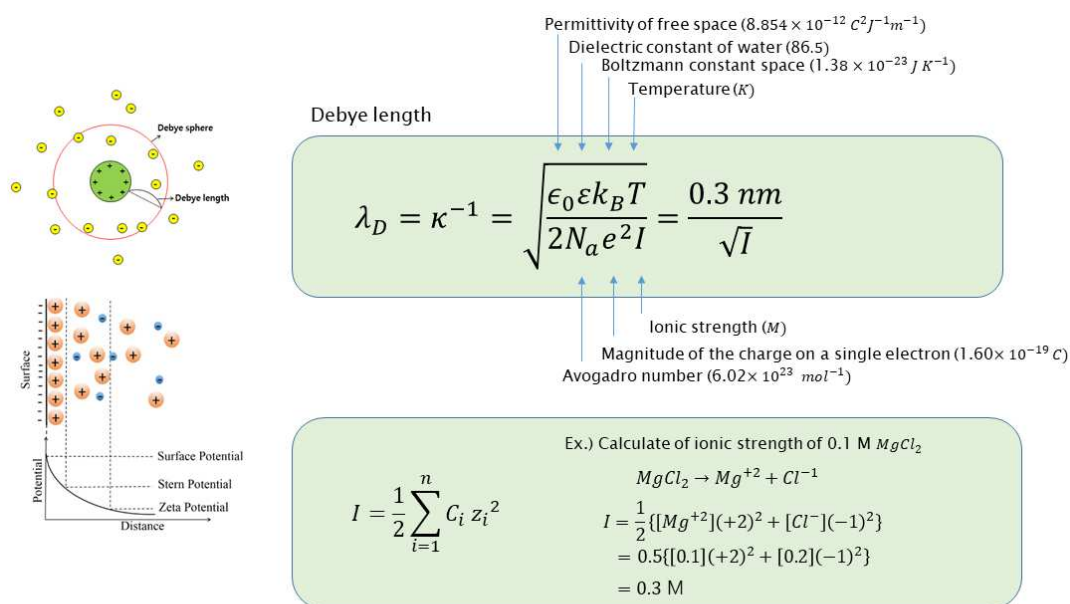


Figure 4.25 Physical constant for the calculation of electrostatic interaction (V_E), van der Waals dispersion interaction (V_D) and hydrophobic interaction (V_H)

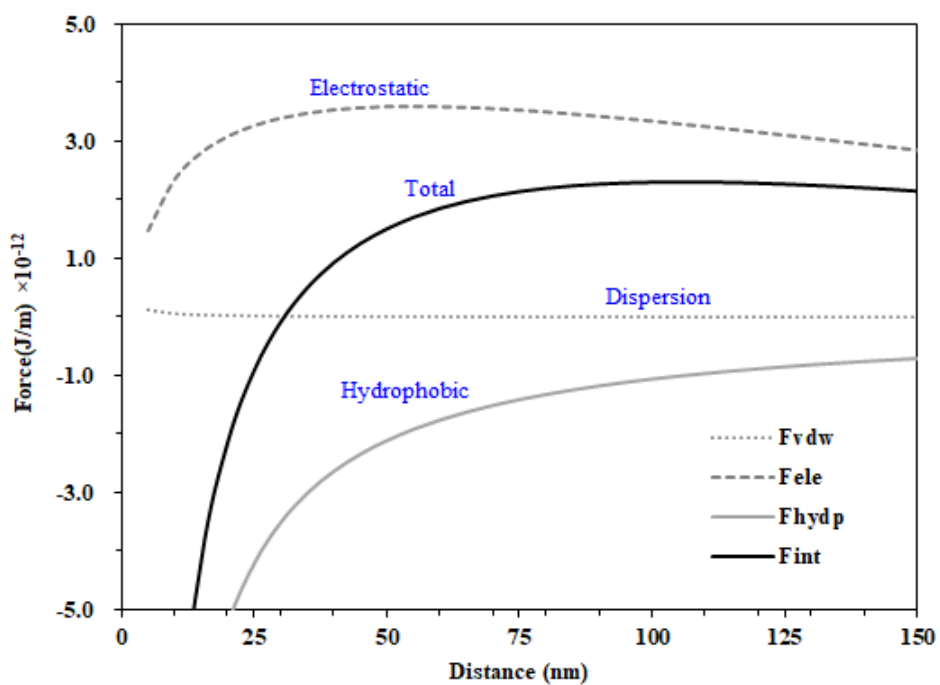


Figure 4.26 Potential energy of bubble-particle interaction as a function of distance

Table 4.13 Model parameters for particle, bubble and water

Particles	Diameter (μm)	Density (kg m^{-3})	Zeta Potential (mV)	Concentration (mg L^{-1})
	600	1050	-20	50
Bubble	Diameter (μm)	Density (kg m^{-3})	Zeta Potential (mV)	Concentration (mg L^{-1})
	16	1.1184	-20	0.25
water	Temp. ($^{\circ}\text{C}$)	Density (kg m^{-3})	Zeta Potential (mV)	Concentration (mg L^{-1})
	25	998	0.0068951	0.003
Physical constants	Hamaker (J)	Hydrophobic (J)	ε (-)	ε_0 (C/volt.m)
	-2.50×10^{-20}	6.30×10^{-19}	86.5	8.85×10^{-12}
	Avogadro (1/mol)	Boltzmann (J K^{-1})	Electron (C)	Wave (m)
	6.02×10^{23}	1.38×10^{-23}	1.60×10^{-19}	1.0×10^{-7}

It has been known that colloidal particles are agglomerated based on the adsorption of hydrogen ions or positive-charged ions (i.e., such as aluminum ions), on negatively-charged surfaces. The coagulation mechanism of PAC is very complex and has several reaction mechanism such as charge neutralization (electrostatic interaction) and complex formation between PAC and alumino precipitates, adsorption, bridge formation and surface precipitation on alumino hydroxide solid precipitate. Prior to sedimentation and flotation measurements, the optimal coagulation conditions were determined. **Figure 4.27** shows the coagulation and sedimentation of powdered biocarbons. To verify the DAF process to float powdered biocarbons, the removal efficiencies was compared in the presence and absence of coagulant. The removal efficiency without coagulant was very low ($< 20\%$), while the efficiency increased with increasing coagulant dose up to 80% by CGS and up to 90% by DAF. It was found that hybrid process consisting of biocarbon adsorption and DAF can be successfully applied to the simultaneous removal of particles and dissolved organics for water and wastewater treatments. For this, further works will be studied for the feasibility of surface modification of PAC and bubble using positively charged chitosan.

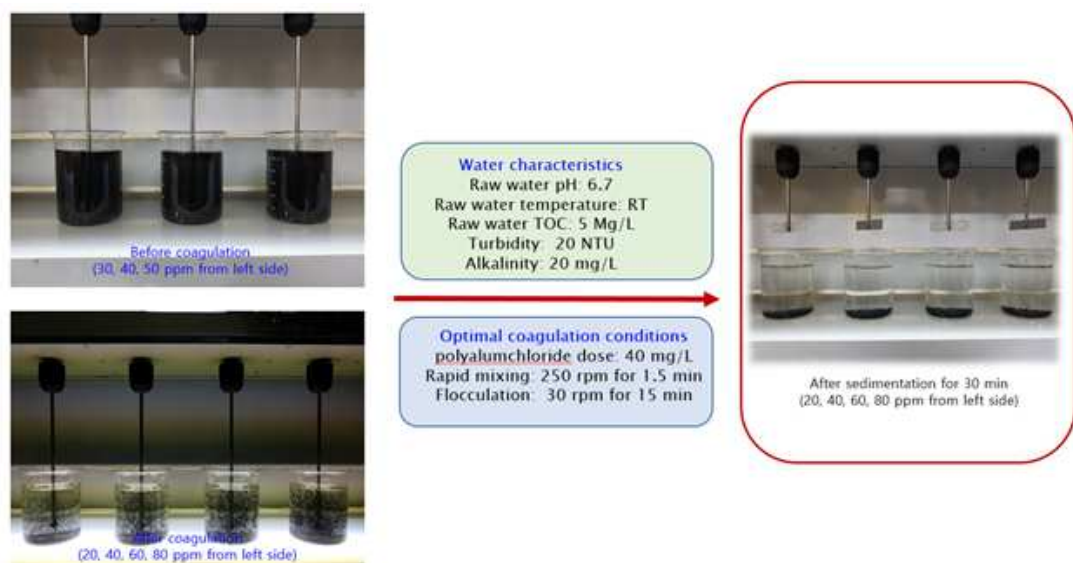


Figure 4.27 Coagulation and sedimentation of powdered biocarbons

Chapter 5

Overall Conclusions

This work has been targeted to design, preparation, characterization and application of hierarchical mesoporous carbon from natural biomass of giant *Miscanthus* and *Chlorella ellipsoidea* for feasibility of utilizing the peroxide-assisted microwave activation. This work provides a simple and sustainable route to obtain hierarchical mesoporous carbons for potential adsorbents and electrode materials from various biomass.

Hierarchical mesoporous carbons from giant *Miscanthus* and *Chlorella ellipsoidea*, one of algae, were successfully prepared by peroxide-assisted microwave activation. The activation was conducted by a simple process of H_2O_2 treatment followed by microwave heating. The activation conditions of H_2O_2 impregnation time and microwave power time were optimized to obtain biocarbon adsorbents with high specific surface area and high adsorption capacity for commercial dye of methylene blue. Pore size distribution, surface morphology and elemental composition of activated bio-carbons were characterized. It is confirmed from the potentiometric titration that peroxide-assisted microwave bio-carbons contain acidic functional groups of oxygen-containing functionalities of carboxyl and hydroxyl groups that may dissociate at higher pH and result in negatively charged surfaces. H_2O_2 impregnation time of 24 h and microwave radiation time of 12 h under the power of 700 W were produced mesoporous biocarbons with narrow pore size distribution. The surface area and average pore size of the hierarchical porous carbon were in the range of $200 \sim 500 \text{ m}^2 \text{ g}^{-1}$ and about 3 nm under different activation conditions. Nitrogen adsorption and desorption are type I isotherm and type H4 hysteresis based on IUPAC classification. The pseudo-second-order model fits the experimental kinetic data very well. The adsorption equilibrium data obtained at different temperatures showed good correlation with the Freundlich isotherm and the maximum adsorption capacity was 30 mg/g. Thermodynamic parameters showed that the adsorption of methylene blue on bio-carbons was feasible,

spontaneous, and endothermic under the studied conditions. Therefore, the prepared biocarbons from giant *Miscanthus* and *Chlorella ellipsoidea* could successfully applied to both adsorbents for the removal of dyes dissolved in water and carbon electrodes for energy storage device.

In DAF process, the total flotation efficiency was highly dependent on the contact efficiency and separation efficiency. The flotation model was formulated by considering the hydrodynamic and surface forces of bubble-particle interaction which is essential in predicting flotation rates. Based on the systematic analysis of experimental and theoretical results, biocarbons can be successfully removed by DAF process. As expected, the flotation efficiencies of powdered biocarbons were enhanced with coagulation dose because of the increase of the zeta potential values. However, the removal efficiency of powdered biocarbons was very low without coagulation. The efficiency increased up to 80% by CGS and to 90% by DAF when polyaluminium chloride was used as a coagulant. The results suggest that the hybrid system of powdered biocarbon adsorption and dissolved air flotation (DAF) processes can be successfully applied for simultaneous removal of particles (i.e., inorganics and algae) and organics dissolved in water.

As a continuous work, the feasibility of surface modification of PAC and bubble using positively charged chitosan will be studied for the simultaneous removal of particles and organics dissolved in water. On the other hand, the higher recovery and selectivity of a flotation process depend on the control of hydrodynamic conditions and surface forces, respectively. The free energy of bubble-particle interaction is the summation of free energy change due to electrostatic interaction, van der Waals interaction, and hydrophobic interaction. The total potential can be calculated from the extended DLVO theory covering the contributions resulted from the hydrophobic interaction between air bubble and particle. For the calculation of the free energy and the total potential, Hamaker constant (H_{132}) and hydrophobic constant (K_{132}) will be studied using AFM technique to measure the hydrophobic surface forces under different conditions.

Reference

1. Wu, H., Zhang, Y., Cheng, L., Zheng, L., Li, Y., Yuan, W., Yuan, X. Graphene based architectures for electrochemical capacitors. *Energy Storage Mater.* 2016, 5, 8 - 32
2. Dai, H. Carbon nanotubes: synthesis, integration, and properties. *Acc Chem Res*, 2002, 35, 1035 - 1044
3. Hummers Jr. W. S., Offeman, R. E. Preparation of graphitic oxide. *J. Am. Chem. Soc.* 1958, 80, 1339 - 1339
4. Shao, Y., El-Kady, M. F., Wang, L. J., Zhang, Q., Li, Q., Wang, H., Mousavi, M. F., Kaner, R. B. Graphene-based materials for flexible supercapacitors. *Chem. Soc. Rev.* 2015, 44, 3639 - 3665
5. Zheng, X., Luo, J., Lv, W., Wang D. W., Yang, Q. H. Two-dimensional porous carbon: synthesis and ion-transport properties. *Adv. Mater.* 2015, 27, 5388 - 5395
6. Jiang, L., Sheng L., Fan, Z. Biomass-derived carbon materials with structural diversities and their applications in energy storage, *Science China Materials*, 61(2) (2018) 133-158
7. Gaddam RR, Yang D, Narayan R, et al. Biomass derived carbon nanoparticle as anodes for high performance sodium and lithium ion batteries. *Nano Energy*, 2016, 26: 346 - 352
8. Yan D, Yu C, Zhang X, et al. Nitrogen-doped CMs derived from oatmeal as high capacity and superior long life anode material for sodium ion battery. *Electrochim Acta*, 2016, 191: 385 - 391
9. Ogale AA, Zhang M, Jin J. Recent advances in carbon fibers derived from biobased precursors. *J Appl Polym Sci*, 2016, 133: 43794
10. Lai F, Miao YE, Zuo L, et al. Biomass-derived nitrogen-doped carbon nanofiber network: a facile template for decoration of ultrathin nickel-cobalt layered double hydroxide nanosheets as high-performance asymmetric supercapacitor electrode. *Small*, 2016, 12: 3235 - 3244
11. Yu H, Zhang W, Li T, et al. Capacitive performance of porous carbon nanosheets derived

- from biomass cornstalk. RSC Adv, 2017, 7: 1067 - 1074
12. Zhou X, Chen F, Bai T, et al. Interconnected highly graphitic carbon nanosheets derived from wheat stalk as high performance anode materials for lithium ion batteries. Green Chem, 2016, 18: 2078 - 2088
 13. Zhang W, Lin H, Lin Z, et al. 3D hierarchical porous carbon for supercapacitors prepared from lignin through a facile template free method. ChemSusChem, 2015, 8: 2114 - 2122
 14. FanYM,SongWL,LiX,etal.Assembly of graphene aerogels into the 3D biomass-derived carbon frameworks on conductive substrates for flexible supercapacitors. Carbon, 2017, 111: 658 - 666
 15. Wu XL, Wen T, Guo HL, et al. Biomass-derived sponge-like carbonaceous hydrogels and aerogels for supercapacitors. ACS Nano, 2013, 7: 3589 - 3597
 16. Tan, X.F., Liu, S.B., Liu, Y.G. Gu, Y.L., Zeng, G.M., HU, X.J., Wang, X. Liu, S.H., Jiang, L.H., Biochar as potential sustainable precursors for activated carbon production: Multiple applications in environmental protection and energy storage, Bioresource Technology 227 (1017) 359-372
 17. Deng, J., Li, M., Wang, Y. Biomass-derived carbon: synthesis and applications in energy storage and conversion. Green Chem. 2016, 18, 4824 - 4854
 18. Wang, J., Nie, P., Ding, B., Dong, S., Hao, X., Dou, H., Zhang, X. Biomass derived carbon for energy storage devices. J. Mater. Chem. A, 2017, 5, 2411 - 2428
 19. Wang-Geun Shim, Chan Kim, Jae-Wook Lee, M.S. Balathanigaimani, Hee Moom, Surface Structural and Energetic Heterogeneity of Carbon Materials Prepared from Corn Grains using Steam and H3PO4-Stream Activations, Surface and Interface Analysis 48 (2016) 82-87
 20. Kwang-Hyun Park, M.S. Balathanigaimani, Wang-Geun Shim, Jae-Wook Lee, Hee Moon, Adsorption Characteristics of Phenol on Novel Corn Grain-based Activated Carbons, Microporous and Mesoporous Materials, 127 (2010) 1-8
 21. M.S. Balathanigaimani, Wang-Geun Shim, Tak-Hee Kim, Sung-June Cho, Jae-Wook Lee, Hee Moon, Hydrogen Storage on Highly Porous Novel Corn Grain-based Activated Carbon Monolith, Catal. Today, 146 (2009) 234-240

22. M.S. Balathanigaimani, Wang-Geun Shim, Min-Joo Lee, Jae-Wook Lee, Hee Moon, Adsorption of Methane on Novel Corn Grain-Based Activated Carbon Monoliths, Microporous and Mesoporous Materials, 119 (2009) 47-52
23. M.S. Balathanigaimani, Wang-Geun Shim, Chan Kim, Jae-Wook Lee, Hee Moon, Surface Structural Characterization of Highly Porous Activated Carbon Prepared from Corn Grains, Surface and Interface Analysis, 41 (2009) 484-488
24. M.S. Balathanigaimani, Wang-Geun Shim, Min-Joo Lee, Jae-Wook Lee, Hee Moon, Adsorption Isotherms of Benzene and Toluene on Corn-based Carbon Monolith at (303.15, 313.15 and 323.15)K, J. Chem. Eng. Data, 53 (2008) 732-736
25. M.S. Balathanigaimani, Wang-Geun Shim, Min-Joo Lee, Chan Kim, Jae-Wook Lee, Hee Moon, Highly Porous Electrodes from Novel Corn Grains-Based Activated Carbons for Electrical Double Layer Capacitors, Electrochemistry Communications, 10 (2008) 868-871
26. M.S. Balathanigaimani, Wang-Geun Shim, Chan Kim, Jae-Wook Lee, Soong-Hyuck Suh, Hee Moon, Charge and Discharge of Methane on Phenol-Based Carbon Monolith, Adsorption, 14 (2008) 525-532
27. Jae-Wook Lee, M.S. Balathanigaimani, Hyun-Chul Kang, Wang-Geun Shim, Chan Kim, Hee Moon, Methane Storage on Phenol-Based Activated Carbon at (293.15, 303.15 and 313.15) K, J. Chem. Eng. Data, 52(1) (2007) 66-70
28. Heo, H. S., Park, H. J., Yim, J. H., Sohn, J. M., Park, J. H., Kim, S. S., Ryu, C. K., Jeon, J. K., Park, Y. K. Influence of operation variables on fast pyrolysis of *Miscanthus sinensis* var. *purpurascens*. *Bioresour. Technol.* 2010, 101, 3672-3677
29. Lee, Y. W., Eum, P. R. B., Ryu, C. K., Park, Y. K., Jung, J. H., Hyun, S. H. Characteristics of biochar produced from slow pyrolysis of *Geodae-Uksae* 1. *Bioresour. Technol.* 2013, 130, 345-350
30. Kim, W. K., Shim, T. Y., Kim, Y. S., Hyun, S. H., Ryu, C. K., Park, Y. K., Jung, J. H. Characterization of cadmium removal from aqueous solution by biochar produced from a giant *Miscanthus* at different pyrolytic temperatures. *Bioresour. Technol.* 2013, 138, 266-270
31. Shim, T. Y., Yoo, J. S., Ryu, C. K., Park, Y. K., Jung, J. H. Effect of steam activation of biochar produced from a giant *Miscanthus* on copper sorption and toxicity. *Bioresour.*

- Technol. 2015, 197, 85-90
32. Zhang, Z., Wang, K., Atkinson, J. D., Yan, X., Li, X., Rood, M. J., Yan, Z. Sustainable and hierarchical porous Enteromorpha prolifera based carbon for CO₂ capture. J. Hazard. Mater. 2012, 229-230, 183-191
 33. Tian, Z., Xiang, M., Zhou, J., Hu, L., Cai, J. Nitrogen and Oxygen-Doped Hierarchical Porous Carbons from Algae Biomass: Direct Carbonization and Excellent Electrochemical Properties. Electrochim. Acta, 2016, 211, 255-233
 34. Tian, Z., Qiu, Y., Zhou, J., Zhao, X., Cai, J. The direct carbonization of algae biomass to hierarchical porous carbons and CO₂ adsorption properties. Mater. Lett. 2016, 180, 162-165
 35. Gao, X., Xing, W., Wang, G., Zhou, S., Liu, Z., Xue, Q., Yan, Z. Superior capacitive performance of active carbons derived from Enteromorpha prolifera. Electrochim. Acta. 2014, 133, 459-466
 36. Zhu, B., Liu, B., Qu, C., Zhang, H., Guo, W., Liang, Z., Chen, F., Zou, R. Tailoring biomass-derived carbon for high-performance supercapacitors from controllably cultivated algae microspheres. J. Mater. Chem. A, 2018, 6, 1523-1530
 37. Foroutan, R., Mohammadi, R., Razeghi, J., Ramavandi, B. Performance of algal activated carbon/Fe₃O₄ magnetic composite for cationic dyes removal from aqueous solutions. Algal Res. 2019, 40, 101509
 38. C. Falco, M. Sevilla, R.J. White, R. Rothe, M.M. Titirici, Renewable nitrogen-doped hydrothermal carbons derived from microalgae, ChemSusChem 5 (2012) 1834-1840

39. Sewu, D. D., Jung, H. S., Kim, S. S., Lee, D. S., Woo, S. H. Decolorization of cationic and anionic dye-laden wastewater by steam-activated biochar produced at an industrial-scale from spent mushroom substrate. *Bioresour. Technol.* 2019, 277, 77-86
40. Shen, Y., Fu, Y. KOH-activated rice husk char via CO₂ pyrolysis for phenol adsorption. *Mater. Today Energy*, 2019, 9, 397-405
41. Singh, J., Bhunnia, H., Basu, S. Adsorption of CO₂ on KOH activated carbon adsorbents: Effect of different mass ratios. *J. Environ. Manage.* 2019, 250, 109457
42. Oginni, O., Singh, K., Oporto, G., Dawson-Andoh, B., McDonald, L., Sabolsky, E. Effect of one-step and two-step H₃PO₄ activation on activated carbon characteristics. *Bioresour. Technol. Rep.* 2019, 8, 100307
43. Elmouwahidi, A., Bailón-García, E., Pérez-Cadenas, A. F., Maldonado-Hódar, F. J., Carrasco-Marín, F. Activated carbons from KOH and H₃PO₄-activation of olive residues and its application as supercapacitor electrodes. *Electrochim. Acta*, 2017, 229, 219-228
44. Ao, W., Mao, X., Kang, Q., Ran, C., Liu, Y., Zhang, H., Gao, Z., Li, J., Liu, G., Dai, J. Microwave assisted preparation of activated carbon from biomass: A review. *Renewable Sustainable Energy Rev.* 2018, 92, 958-979
45. Nair, V., Vinu, R. Peroxide-assisted microwave activation of pyrolysis char for adsorption of dyes from wastewater. *Bioresour. Technol.* 2016, 216, 511-519
46. Liew, R. K., Azwar, E., Yek, P. N. Y., Lim, X. Y., Cheng, C. K., Ng, J. H., Jusoh, A., Lam, W. H., Ibrahim, M. D., Ma, N. L., Lam, S., S. Microwave pyrolysis with KOH/NaOH mixture activation: A new approach to produce micro-mesoporous activated carbon for textile dye adsorption. *Bioresour. Technol.* 2018, 266, 1-10
47. Chen, S., Chen, Q., Xia, H., Zhag, L., Peng, J., Lin, G., Liao, Z., Jiang, X., Zhag, Q., Microwave one-pot production of ZnO/Fe₃O₄/activated carbon composite for organic dye removal and the pyrolysis exhaust recycle., *J. Cleaner Production* 188 (2018) 900-910
48. Ge, Z., Wu, Z., Wu, Z., Yan, Y., Cravotto, G. Ye, B.C., Microwave-assisted modification of activated carbon with ammonia for efficient pyrene adsorption, *J. Industrial and Engineering Chemistry* 39 (2016) 27-36
49. Schulze, H. J. *Physico-Chemical Elementary Processes in Flotation*, Elsevier, 1984.

50. Cook, D., Newcombe, G., Sztajn bok, P., The application of powdered activated carbon for MIB and Geosmin removal: predicting PAC doses in four raw waters. *Wat. Res.* 2001, 35, 1325-1333
51. Graham, M., Summers, R.,s Simpson, M., Maceleod, B. Modeling equilibrium adsorption of 2-methylisoborneol and geosmin in natural water. *Wat. Res.* 2000, 34, 2291-2300
52. Chen, Y. M., Liu, J. C., Ju, Y. H. Flotation removal of algae from water, *Colloids and Surfaces B: Biointerfaces*, 1998, 12, 49-55
53. Bourgeois, J. C., Walsh, M. E., Gagnon, G. A. Treatment of drinking water residuals: comparing sedimentation and dissolved air flotation performance with optimal cation ratios. *Wat. Res.* 2004, 38, 1173-1182
54. Dong-Heui Kwak, Seung-Joon Yoo, Heung-Joe Jung, Sun-Beum Kwon, Eun-Ji Lee, Chan-Hee Won, Jae-Wook Lee, Rise Velocity Verification of Bubble-Floc Agglomerates Using Population Balance in DAF Process, *J. Water Supply: Research and Technology - AQUA*, 58(2) (2009) 85-94
55. Kwak and Lee et al., Simultaneous Removal of Algae and Their Secondary Algal Metabolites from Water by Hybrid System of DAF and PAC Adsorption, *Sep. Sci. Tech.* 43 (2008) 113
56. D. H. Kwak, S. J. Kim, H. J. Jung, C. H. Won, S. B. Kwon, H. W. Ahn, J. W. Lee, Removal of Clay and Blue-Green Algae Particles through Zeta Potential and Particle Size Distribution in Dissolved Air Flotation Process, *Water Science and Technology: Water Supply*, 6(1) (2006) 95-103
57. Heung-Joe Jung, Jae-Wook Lee, Do-Young Choi, Seong-Jin Kim, Dong-Heui Kwak, Flotation Efficiency of Activated Sludge Flocs using Population Balance Model in Dissolved Air Flotation, *Korean J. Chem. Eng.*, 23(2) (2006) 271-278
58. D. H. Kwak, H. J. Jung, S. J. Kim, C. H. Won, J. W. Lee, Separation Characteristics of Inorganic Particles from Rainfalls in Dissolved Air Flotation: A Korean Perspective, *Separation Science and Technology*, 40 (2005) 3001-3016
59. J. W. Lee, S. P. Choi, R. Thiruvengkatachari, W. G. Shim, H. Moon, Submerged microfiltration membrane coupled with alum coagulation/powdered activated carbon

- adsorption for complete decolorization of reactive dyes, *Water Research*, 40 (2006) 435-444
60. Lagergren, S., Svendka, B.K., Zur theorie der sogenannten adsorption gelöster stoffe. *Veternskapsakad Handlingar* 24 (1898) 1-39
 61. Ho, Y.S., Adsorption of heavy metals from waste streams by peat, Ph.D. Thesis, University of Birmingham, Birmingham, UK (1995)
 62. Aharoni, C., Tompkins, F.C., In: Eley, D.D., Pines, H., Weisz, P.B. (Eds.), *Adv. Catal. Related Subj.* 21, Academic Press New York (1970)
 63. Langmuir, I., The constitution and fundamental properties of solids and liquids, *J. Am. Chem. Soc.* 38 (1916) 2221-2295
 64. Freundlich, H.M.F., Over the adsorption in solution. *J. Phys. Chem.* 57 (1906) 385-471
 65. M.M. Dubinin, L.V. Radushkevich, The equation of the characteristic curve of activated charcoal, in: *Proceedings of the Academy of Sciences URSS Phys. Chem. Sect.*, 55, 1947, p. 331
 66. S.S. Dubey, R.K. Gupta, Removal behavior of Babool bark (*Acacia nilotica*) for submicro concentrations of Hg^{2+} from aqueous solutions: a radiotracer study, *Sep. Purif. Technol.* 41 (2005) 21 - 28
 67. F. Helfferich, *Ion Exchange*, McGraw-Hill, New York, 1962.
 68. M.S. Onyango, Y. Kojima, O. Aoyi, E.C. Bernardo, H. Matsuda, Adsorption equilibrium modeling and solution chemistry dependence of fluoride removal from water by trivalent-cation-exchanged zeolite F-9, *J. Colloid Interface Sci.* 279 (2004) 341 - 350.
 69. K.K. Singh, R. Rastogi, S.H. Hasan, Removal of Cr(VI) from wastewater using rice bran, *J. Colloid Interface Sci.* 290 (2005) 61 - 68
 70. J.M. Smith, H.C. Van Ness, M.M. Abbott, *Introduction to Chemical Engineering Thermodynamics*, 7th ed., McGraw-Hill, Singapore, 2005.
 71. G. McKay, The adsorption of basic dye onto silica from aqueous solution-solid diffusion model, *Chem. Eng. Sci.* 39 (1984) 129 - 138
 72. R. Ileri, F. Mavituna, S. Dimokopoulos, Removal of low level lead ions from aqueous solutions by dead cells of *Rhizopus arrhizus*, in: *Proceedings of the AWT'98 on Advanced Waste-water treatment, Recycle, Reuse, Milans, Holy*, 14 - 16 September, 1998, pp.

1079 - 1082

73. G. McKay, M.J. Bino, Adsorption of pollutants from wastewater onto activated carbon based on external mass transfer and pore diffusion, *Water Res.* 22 (1988) 279 - 286.
74. A. Selatnia, A. Boukazoula, N. Kechid, M.Z. Bakhti, A. Chergui, Y. Kerchich, Biosorption of lead (II) from aqueous solution by a bacterial dead *Streptomyces rimosus* biomass, *Biochem. Eng. J.* 19 (2004) 127 - 135
75. K. Urano, H. Tachikawa, Process development for removal and recovery of phosphorus from wastewater by new adsorbent. II. Adsorption rates and breakthrough curves, *Ind. Eng. Chem. Res.* 30 (1991) 1897 - 1899
76. R.H. Yoon, The role of hydrodynamic and surface forces in bubble-particle interaction, *Int. J. Miner. Process.* 58 (2000) 129-143
77. Yoon, R.H. Luttrell, G.H. The effect of bubble size on fine particle flotation, *Miner. Process. Extr. Metall. Rev.* 5 (1989) 101-122
78. Leppinen, D. M. (1999) Trajectory analysis and collision efficiency during microbubble flotation. *Journal of Colloid and Interface Science*, 212, 431-442
79. Leppinen, D. M. (2000) A kinetic model of dissolved air flotation including the effects of interparticle forces. *Journal of Water Supply: Research and Technology-Aqua*, 49(5), 259-268
80. Okada, K., Akagi, Y., Kogure, M., Yoshioka, N., Analysis of particle trajectories of small particles in flotation when the particles and bubbles are both charged. *Can. J. Chem. Eng.*, 1990, 68, 614-621
81. Fukushi, K., Tambo, N., Matsui, Y. A kinetic model for dissolved air flotation in water and wastewater treatment. *Wat. Sci. Tech.* 1995, 32, 37-47
82. Edzwald, J. K. (2010) Dissolved air flotation and me, *Water Research*, 44, 2077-2106.
83. Edzwald, J. K. (1995) Principles and applications of dissolved air flotation. *Wat. Sci. & Technol.*, 31(3-4), 1-25
84. Li, D.P. and Huang, Y. (2010) Sedimentary phosphorus fractions and bioavailability as influenced by repeated sediment resuspension. *Ecological Engineering*, 36(7), 958-962
85. Matsui, Y., Fukushi, K. and Tambo, N. (1998) Modeling, simulation, and operational

- parameters of dissolved air flotation. *Journal of Water Supply: Research and Technology-Aqua*, 47(1), 9-20
86. Tambo, N., Matsui, Y. and Fukushima, K. (1986) A kinetic study of dissolved air flotation, *World Congress of Chemical Engineering*, Tokyo.
 87. M.S. Kim, D.H. Kwak, Role and applicability of bubble flotation model in sediment remediation in natural water systems, *Separation and Purification Technology* 222 (2019) 309-320
 88. J. Haarhoff, J.K. Edzwald, Dissolved air flotation modelling: insights and shortcomings, *J. Water Supply: Res. Technol.-Aqua* 53 (3) (2004) 127 - 150
 89. Derjaguin, B.V., 1934. Friction and adhesion: IV. The theory of adhesion of small particles. *Kolloid-Z.* 69, 155 - 164
 90. W. A. Ducker, T. J. Senden, R. M. Pashley, Direct measurement of colloidal forces using an atomic force microscope, *Nature*, 353, (1991) 239 - 241
 91. Israelachvili, J.N., Pashley, R.M., 1988. The hydrophobic interaction is long range, decaying exponentially with distance. *Nature*, 300, (1982) 341 - 342
 92. Rabinovich, Y.I., Yoon, R.-H., 1994. Use of atomic force microscopy for the measurements of hydrophobic forces. *Colloid Surf.* 93, 263 - 273
 93. Yoon, R.-H., Aksoy, B.S., 1999. Hydrophobic forces in thin water films stabilized by dodecylammonium chloride. *J. Colloid Interface Sci.* 211, 1 - 10
 94. Yoon, R.-H., Luttrell, G.H., 1989. The effect of bubble size on fine particle flotation. *Miner. Process. Extr.Metall. Rev.* 5, 101 - 122
 95. Yoon, R.-H., Mao, L., 1996. Application of extended DLVO theory: IV. Derivation of flotation rate equation from first principles. *J. Colloids Interface Sci.* 181, 613 - 626
 96. Yoon, R.-H., Ravishankar, S.A., 1993. Application of extended DLVO theory: III. Effect of octanol on the long-range hydrophobic forces between deodecylamine-coated mica surfaces. *J. Colloids Interface Sci.* 165, 1 - 10
 97. Yoon, R.-H., Ravishankar, S.A., 1996. Long-range hydrophobic forces between mica surfaces in dodecylammonium chloride solutions in the presence of dodecanol. *J. Colloids Interface Sci.* 179, 391 - 402

98. Yoon, R.-H., Luttrell, G.H., Adel, G.T., Mankosa, M.J., 1989. Recent advances in fine coal flotation. In: Chander, S. Ed., *Advances in Coal and Mineral Processing Using Flotation*, Chap. 23. Society of Mining Engineers, Littleton, CO, pp. 211 - 218
99. Yoon, R.-H., Flinn, D.H., Rabinovich, Y.I., 1997. Hydrophobic interactions between dissimilar surfaces. *J. Colloids Interface Sci.* 185, 363 - 370
100. Chen, C. Huang, W., Aggregation kinetics of nanosized activated carbons in aquatic environments, *Chem. Eng. J.* 313 (2017) 882-889
101. Liu, Y., Hu, Y. Yang, C., Chen, C. Huang, W., Dang, Z., Aggregation kinetics of UV irradiated nanoplastics in aquatic environments, *Water Research* 163 (2019) 114870
102. Morra, M., Occhiello, E., Garbassi, F., Effect of surface treatment on the Hamaker constant of intermediate modulus carbon fibers, *Colloid Polymer Science* 270 (1992) 58-63
103. Maurer, S., Mersmann, A., Peukert, W., Henry coefficients of adsorption predicted from solid Hamaker constants, *Chemical Engineering Science* 56 (2001) 3443-3453
104. Chen, K.L., Elimelech, M., Aggregation and deposition kinetics of fullerene (C60) nanoparticles, *Langmuir* 22 (2006) 10994-1101
105. Israelachvili, J.N., *Intermolecular and surface force: revised, third ed.* (2011), Academic press, London, U.K.
106. Ottewill, R.H., Shaw, J.N., Stability of monodisperse polystyrene latex dispersions of various sizes, *Dis. Faraday Soc.* 42 (1966) 154-163
107. Visser, J., On Hamaker constants: a comparison between Hamaker constants and Lifshitz-van der Waals constants, *Adv. Colloid Interface Sci.* 3 (1972) 331-363.

국문 초록

천연바이오매스 기반 다공성 탄소소재 개발 및 응용

김 석 중

지도교수 : 이 재 욱

화학공학과

조선대학교 대학원

지속가능한 탄소 전구체로서 바이오 폐기물로부터 얻은 바이오탄소는 활성탄소를 생산하는데 많은 관심을 받고 있다. 일반적으로 활성화 공정을 통해 조절된 물리적 화학적 특성을 지닌 활성탄소는 수처리, 이산화탄소 회수 및 에너지 저장 등과 같은 다양한 응용분야에 적용되고 있다. 바이오 매스의 성분과 종류 그리고 기존 방식의 열처리 및 마이크로웨이브 열처리 공정을 통한 활성화 조건은 탄화 및 활성화 공정의 주요 조절 변수로 작용한다. 이렇게 제조된 활성탄소는 기존 활성탄소에 비해 저렴하고 친환경적인 탄소 물질로서 다양한 분야에서 활발히 응용되리라 예상된다.

본 학위논문에서는 거대역새 및 조류와 같은 바이오매스를 이용하여 높은 표면적을 지니면서 세공크기 조절이 가능한 규칙적인 메조세공의 탄소물질을 제조하였다. 활성화 공정은 바이오 매스를 과산화수소로 처리한 후, 마이크로웨이브를 이용하여 가열하였다. 최적의 과산화수소수 담지 시간 및 마이크로 웨이브 조사 시간은 메틸렌블루 흡착용량을 통해 최적화 하였다. 제조된 샘플의 표면적, 세공크기(분포) 및 표면 형태는 TG, SEM, XRD, FTIR, BET 및 zeta potential 측정을 통해 조사하였다. 제조된 다공성 탄소체의 흡착특성을 고찰하기 위해 메틸렌블루 염료에 대한 흡착평형 및 속도 데이터를 확보한 후, 흡착등온선(Langmuir, Freundlich)과 pseudo-second-order 모델을 이용하여 그 특성을 조사하였다. 온도 변화에 따른 흡착등온선을 이용하여 열역학적 매개변수 (ΔG^0 , ΔH^0 , ΔS^0)를 구하여 확인한 결과, 제조된 바이오 흡착제 상에서 염료의 흡착은 자발적인 흡착 및 흡열 과정임을 확인하였다. 한편 탄소체의 전기화학특성은 cyclic voltametry 및 impedance 측정을 통해 조사하였다. 그 결과 마이크로 웨이브를 통해 제

조된 탄소 흡착제는 높은 흡착용량 및 우수한 전기적 특성을 지님을 확인할 수 있었다.

조류입자(*anabaena* sp. and *microcystis* sp.) 및 조류의 이차대사산물인 용존 유기물(2-methylisoborneol and geosmin)을 동시에 제거하기 위한 연구로서, 분말활성탄 흡착 및 DAF(dissolved air flotation) 결합공정에 관해 조사하였다. 이를 위해 결합공정에 관한 연구이전에 탄소 흡착제 상에서 이차 대사산물의 흡착 평형 및 속도에 관해 조사하였다. 조류 및 PAC의 부상효율은 제타 포텐셜 측정을 통해 평가하였다. 제타 포텐셜은 전기이중층을 이해하는 데 매우 중요한 정보일 뿐만 아니라 응집 효율을 해석하는데도 사용된다. 물 속에 용해된 이차대사산물(2-methylisoborneol and geosmin)을 흡착한 바이오 탄소체의 부상 효율에 관해 조사하였다. 이를 위해 다양한 조건에서 탄소체 입자(PAC)와 조류입자(*anabaena* sp. and *microcystis* sp.)의 제타전위 변화를 측정하고 부상 분리효율에 어떻게 영향을 미치는지를 조사하였다. 본 연구에서는 증류수, 계곡수 및 저수지의 수질 특성과 응집제의 투여량과 같은 다양한 실험조건에서 제타 포텐셜의 변화를 측정하였다. 그 결과 제타 포텐셜은 수질의 특성 및 응집조건에 매우 민감함을 확인 할 수 있었다. 특히 두 종류의 조류(*anabaena* sp. and *microcystis* sp.)의 제타 포텐셜은 응집제의 투여량에 크게 바뀐다는 사실을 알 수 있었다. 따라서 조류 입자를 제거하기 위해서는 매우 조심스러운 제타 포텐셜 조절이 요구됨을 알 수 있었다. 버블과 플럭의 충돌효율은 DLVO 이론과 궤도분석 방법으로 구성된 모델로 잘 묘사됨을 확인할 수 있었다. 특히 흥미로운 사실은 PAC 입자와 버블로 이루어진 플럭 또한 DAF 공정으로 효과적으로 부상될 수 있음을 알았다. 즉 조류 입자와 이들의 이차대사 산물이 물속에 용해된 유기물들의 동시 제거는 흡착-DAF 결합공정을 통해 가능하다는 것을 알 수 있었다.